Design Of Husky Carbon V.3

A Thesis Presented

by

Yogi Shah

to

The Department of Electrical and Computer Engineering

in partial fulfillment of the requirements

for the degree of

Master of Science

in

Robotics

Northeastern University

Boston, Massachusetts

December 2025

To my family.

Contents

List of Figures

List of Tables

List of Acronyms

M4 Multi-Modal Mobility Morphobot.

CAD Computer aided design.

PIP Print In Place

Acknowledgments

I extend my sincere gratitude to all the members of the Silicon Synapse Lab at Northeastern University for their support throughout my thesis journey. I am especially grateful to Prof. Alireza Ramezani, my primary advisor, for his technical guidance, mentorship, and continuous encouragement. His insights played a pivotal role in shaping both the direction and depth of this work.

I would also like to acknowledge Chenghao Wang (Ph.D. candidate) for his extensive support in setting up the robot's control architecture and for his valuable feedback during the writing and presentation phases of this thesis. I am thankful to Arjun Viswanathan (M.S. student) for his assistance with code implementation, Tengyi Zhang (M.S. student) and Sonia Robinson (undergrad) with design aesthetics, which accelerated the prototyping process and brought robot to life.

Special thanks are due to both Chenghao Wang and Prof. Ramezani for their guidance in drafting this thesis and preparing the final defense presentation.

Lastly, I am deeply grateful to my parents, whose moral and financial support enabled me to pursue my graduate education at Northeastern University. Their belief in me has been the foundation of this accomplishment.

Abstract

Design Of Husky Carbon V.3

by

Yogi Shah

Master of Science in Robotics

Northeastern University, December 2025

Dr. Alireza Ramezani, Adviser

This thesis presents the mechanical design, fabrication, assembly, and experimental validation of Husky V3, a significantly improved iteration of the Husky robot family—a multi-modal ground-aerial platform that addresses multi-locomotion integration through thrust modulation and posture control. The quadruped architecture employs appendage repurposing capable of transitioning between legged and aerial locomotion modes. This work addresses critical compliance and structural deficiencies encountered in Husky Carbon V2, where excessive torso and link flexion compromised flight safety and control stability. The redesign prioritizes structural rigidity through comprehensive component optimization, substantial weight reduction, and integrated wire routing embedded within the leg structure to ensure safe operation and aesthetic presentation. Key innovations include a novel print-in-place (PIP) articulated ankle joint design that eliminates multi-part assembly complexity and bearing installation requirements, replacing them with a single-piece revolute joint. Additionally, custom bearing-embedded motor casing designs facilitate clean wire routing while maintaining structural integrity. Experimental validation demonstrates that these design refinements successfully eliminate structural flexion, reduce system mass for improved thrust-to-weight ratio, and establish Husky V3 as a robust, practical platform for multi-modal locomotion research.

Chapter 1

Introduction

1.1 Background and Motivation

Current paradigms in autonomous mobility have increasingly specialized platforms: ground-based robots excel in traversing complex terrain with extended operational duration and payload capacity, while aerial vehicles provide rapid transit and access to otherwise unreachable environments. However, this specialization creates a critical operational gap in scenarios requiring both long-duration presence and the ability to overcome significant environmental obstacles. Integrated legged-aerial systems that combine the terrain adaptability of quadrupedal locomotion with aerial propulsion represent a promising solution to this dichotomy [15], [31]. Yet, such hybrid platforms remain largely unexplored due to fundamental conflicts in design requirements: powerful actuators and rugged structures needed for terrestrial locomotion directly compromise the lightweight, efficient design demanded by aerial mobility [15]. The mechanical integration and control complexity of seamless legged-aerial locomotion significantly exceeds that of conventional single-modal platforms. Consequently, the design and development of robots capable of unified legged-aerial locomotion remains an under-addressed research challenge.

Legged locomotion systems demonstrate distinctive advantages in obstacle traversal and terrain adaptation through their integrated agility and dynamic balancing capabilities [29], [2]. Beyond conventional structured obstacles such as street curbs, staircases, and debris fields, these systems prove particularly valuable on unstructured natural terrains characterized by inclines, rocky composition, and muddy substrates, where traditional wheeled locomotion proves inadequate [12], [10],[35]. Recent advances in learning-based control have enabled quadrupedal robots to achieve remarkable robustness across challenging natural environments, demonstrating zero-shot general-

ization to deformable terrains such as mud and snow, dynamic footholds like rubble, and overground impediments such as thick vegetation [29], [39], [73]. These developments underscore the critical role of proper footholds and body posture control in enabling quadrupeds to navigate complex terrain [1], [19].

To overcome inherent limitations of single-mode locomotion, researchers have increasingly explored multimodal systems that combine complementary movement strategies. A seminal example is LEONARDO (LEgs ONboARD drOne), a bipedal robot developed at Caltech that seamlessly integrates bipedal walking with distributed electric propeller thrusters [25]. LEONARDO demonstrates synchronized control of legs and aerial propulsion to achieve complex maneuvers—including slackline walking, skateboarding, and dynamic balancing—that are challenging for purely terrestrial or aerial platforms [25]. This breakthrough platform exemplifies how multimodal locomotion enables robots to adaptively select movement strategies based on environmental demands, improving efficiency and operational capability across diverse terrains.

Further advancing this paradigm, recent work has extended thruster-assisted capabilities to quadrupedal platforms. The M4 (Multi-Modal Mobility Morphobot) robot, published in Nature Communications, utilizes diverse forms of ground locomotion, including quadrupedal walking combined with thruster-based aerial mobility and morphing structures to negotiate collapsed structures and rough terrain [36]. Similarly, work on micro quadruped-quadrotor hybrids demonstrates that coordinated motion control schemes leveraging bio-inspired central pattern generation (CPG) controllers enable seamless terrestrial-to-aerial transitions, with stable walking and flying configurations in complex environments [74]. These platforms have demonstrated particular promise for search-and-rescue operations and multi-elemental disaster response scenarios [31].

The integration of aerial capabilities with legged systems necessitates careful consideration of actuator selection and morphological design. Distributed propeller-based thrusters offer compact, powerful, and modular solutions compared to traditional rigid rotorcraft [25], [24],[40]. Additive manufacturing has emerged as a transformative approach for rapid prototyping and fabrication of complex legged structures, enabling the integration of rigid and compliant elements in novel configurations [9][5] [70]. Recent advances in 3D printing technology—including multi-material fabrication and the integration of actuator systems—have enabled researchers to design and deploy soft and hybrid robotic platforms with unprecedented design flexibility [11], [53]. These manufacturing approaches facilitate rapid iteration and enable deployment of research platforms suitable for challenging field environments [13].

Exemplifying this capability, the Crater Observing Bioinspired Rolling Articulator (CO-

BRA) [45] represents a bio-inspired multimodal snake robot engineered to navigate extreme lunar terrain through morphing locomotion strategies. COBRA achieves terrain adaptability by transitioning between two distinct locomotion modes: sidewinding for traversing flat and low-incline surfaces, and tumbling[21] locomotion where the robot forms a circular barrel configuration by linking its head and tail for rapid movement on steep slopes[46][44][47][48]. This morphing capability—enabled by additive manufacturing of modular articulated segments—demonstrates how biologically-inspired design combined with advanced fabrication techniques creates platforms capable of autonomous operation in harsh, unpredictable environments[50][20][51]. Equipped with onboard computation, stereo vision, inertial measurement, and joint feedback systems[21], COBRA validates that 3D-printed segmented architectures can integrate sensing and actuation while maintaining structural robustness for field deployment in extreme conditions such as lunar crater navigation, establishing a precedent for manufacturing-enabled morphing platforms applicable to terrestrial exploration and dynamic environment adaptation.

Building upon the success of morphing locomotion in terrestrial and extreme environment robotics, research has increasingly focused on achieving dynamic morphing in aerial platforms. This work presents Aerobat, a bioinspired flapping drone that exemplifies advanced morphing capabilities through coordinated actuation of 14 body joints in a tail-less configuration [42][52][61][41]. Unlike conventional flapping wing designs that rely on open-loop stability and fixed wing geometry, Aerobat integrates mechanical intelligence with closed-loop control to enable dynamically versatile wing conformations, allowing real-time adaptation to aerodynamic demands and environmental disturbances. The key innovation in Aerobat's design framework lies in the strategic deployment of low-power primer actuators that produce significant flight control authority through the robot's computational morphing structures, achieving substantial control effects despite minimal actuation power and weight penalty[60][43][57][58]. By hosting numerous lightweight primers distributed across the body, Aerobat demonstrates that morphing-based flight control can be achieved without sacrificing platform agility or energy efficiency, fundamentally challenging the paradigm of fixed-geometry aerial platforms. Aerobat's successful untethered flight validation with joint motion regulation establishes that bioinspired morphing is not limited to terrestrial locomotion but extends to aerial domains, where coordinated appendage reconfiguration and distributed low-power actuation enable flight modes impossible with conventional rigid-wing designs, providing a complementary perspective to ground-based morphing platforms like Cobra and informing the design of hybrid terrestrial-aerial systems[55][59][16].

Our research trajectory began with Harpy [40] [6][30][25][37], a successful bipedal thruster-

assisted platform that demonstrated the feasibility of aerial-augmented locomotion by seamlessly integrating flight capabilities with dynamic bipedal walking through coordinated thrust vectoring and leg dynamics. Harpy's success in morphing between distinct locomotion modes inspired a fundamental shift in our research philosophy: rather than designing task-specific subsystems, we could architect platforms where individual components serve multiple functional roles, enabling locomotion plasticity through intelligent repurposing. This vision evolved into M4—the Multi-Modal Mobility Morphobot[36]—a wheeled platform equipped with repurposable thrusters that dynamically transition between ground-based mobility, autonomous flight[62], and hybrid trotting locomotion by strategically reallocating thrust vector direction and magnitude[33]. Building upon Harpy's distributed thruster integration, M4 demonstrates that aerial-augmented locomotion extends beyond traditional bipedal or quadrupedal structures: by decoupling propulsion from locomotion mode, a wheeled platform with intelligent thruster reallocation achieves the agility of aerial vehicles, the stability of ground robots, and novel hybrid gaits through coordinated modulation of wheel torque and thrust vectoring, establishing a new paradigm for adaptive robotics where locomotion plasticity emerges from component repurposing rather than mechanical reconfiguration[49]. Building on this foundation, we extended these thruster capabilities to quadrupedal systems, which led to the inception of the Husky robot family—a morpho-functional quadruped equipped with thrusters enabling flight and jetpack-assisted maneuvers.

The first iteration, Husky Carbon[63][28], was specifically engineered to address the demanding requirements of search and rescue operations and multi-elemental disaster response scenarios. In such environments, robots must navigate unpredictable weather, including collapsed structures, floods, and unstable wind patterns, while maintaining the agility to access confined spaces and the capability to rapidly traverse open areas [56][27][26]. Fabricated with reinforced thermoplastic material through additive manufacturing, Husky Carbon integrates morphing leg structures with coordinated flight dynamics and shoulder-mounted thrusters to create a unified legged-aerial platform. Inspired by canine leg structure and aerial vehicle agility, this design delivers safe, agile ground-based locomotion combined with rapid aerial maneuvering, enabling a versatile quadrupedal platform capable of operating effectively across diverse disaster environments.

This vision evolved further with Husky Carbon V2, which fundamentally addresses the limitations encountered in the previous iteration by tackling the challenges of short flight duration, weight constraints, and complex actuators that hindered precise control and system reliability. These practical constraints motivated a comprehensive redesign focused on simplicity, modularity, and enhanced operational efficiency. Husky V2 prioritizes a streamlined design approach, utilizing

off-the-shelf actuators and components to maintain hardware simplicity while achieving the same versatile capabilities. Unlike conventional multi-modal robots that rely on distinct appendages for each locomotion task, Husky V2 achieves functional redundancy with minimal overhead through shared, reconfigurable leg structures. This design philosophy—emphasizing structure repurposing and integrating perception[68][69] with terrain-aware control—addresses the inherent complexity of integrated hardware and control strategies while maintaining compactness and embeddedness, enabling deployment in search and rescue operations, environmental monitoring, and autonomous exploration missions.

1.2 Contributions and Thesis Outline

This thesis documents the mechanical design and development of Husky V3, representing a substantial advancement over its predecessor, Husky Carbon V2, with significant improvements in weight reduction and operational efficiency. The primary contributions of this research are outlined below:

Mechanical Design Contributions

- **Lightweight and robust:** The total robot weight was reduced by $\tilde{2}0\%$ (from 6.7kg Xkg), resulting in a **lift-to-weight ratio of 2.67:1**
- **Structural Strength**: departing from the previous flexible component design, this version adopts a more rigid and structurally robust configuration.
- **Component optimization:**
  - The torso design eliminates structural flexion for enhanced rigidity.
  - Foot and ankle assemblies have been removed to reduce mass and complexity.
  - Thrust bearings at the ankle joint have been replaced with a 3D printed pin-in-place (PIP) revolute joint design, reducing component count and weight.
  - Fastener standardization has been implemented to minimize variation in sizes and lengths, simplifying assembly and maintenance.

Platform flexibility & Prototyping

- **Embedded wire architecture:** based on the previous design complexity, this platform has been designed with channels and custom motor casings with part embedding for wire routing to have seamless morphing and flight
- **Easy Part Replacement:** designed to enable rapid component replacement if damaged during experiments
- **In-house Prototyping:** Employing iterative design refinement and economical multi-material 3D printing, this prototype facilitates evaluation of structural robustness and mechanical failure boundaries.

Outline of This Thesis This report is structured as follows:

1. **Introduction and Background** – A review of the Husky V2 platform and its bio-inspired goals
2. **Design and Methodology** – Detailed documentation of the mechanical architecture, material selection, joint design, and embedded wire routing
3. **Prototyping and Assembly Process** – An overview of the fabrication, integration, and testing methods
4. **Comparative Analysis** – Performance improvements over previous versions
5. **Conclusion and Future Work** – Reflections on system capabilities and a road map for autonomous multi-modal operation

Chapter 2

Literature Review

The design of advanced legged robots requires careful integration of mechanical architecture, actuator systems, and structural optimization to achieve robust multi-modal locomotion. This literature review examines the state of the art in quadrupedal robot design, with particular focus on actuator selection, joint design, structural optimization, fabrication methods, and hybrid legged-aerial platforms—all critical to the development of Husky V3.

Actuator design represents a fundamental design choice that directly influences locomotion performance, control bandwidth, and system reliability. The challenge in designing actuators for legged robots is achieving high torque density while maintaining impact robustness and minimizing mass—requirements that traditional manufacturing-oriented actuators fail to satisfy [72]. [72] introduces the proprioceptive actuation paradigm implemented in the MIT Cheetah, demonstrating that high-bandwidth force control can be achieved through collocated force sensing at motor currents without requiring external force sensors or series elastic elements. This approach uses high-torque-density motors with single-stage backdriveable planetary gearboxes, enabling the robot to control contact interactions at the feet during dynamic conditions including high-speed locomotion exceeding 13 mph. The proprioceptive framework provides impact mitigation naturally through motor backdrivability, eliminating the need for additional compliance elements that would add mass and complexity.

Building directly on this foundation, [7] extends proprioceptive actuation to all three degrees of freedom per leg in the MIT Cheetah 3, compared to only hip and knee actuation in prior generations. This architectural improvement enables true 3D locomotion control without external force sensors, achieved through identical high-torque-density motors at all joints and co-axial joint placement that reduces structural complexity. The resulting platform demonstrates a cost of trans-

port (CoT) of 0.45 during trotting—approaching biological efficiency—and exhibits reactive terrain adaptation capability enabling blind stair climbing.

The principles of actuator design extend beyond proprioceptive control to broader efficiency considerations. [54] develops systematic design principles for energy-efficient legged locomotion, establishing how to minimize three primary energy dissipation modes: Joule heating in motors, transmission losses through gearboxes, and interaction losses at ground contact. By integrating motor selection, gearbox design, and low-inertia leg structures, the MIT Cheetah achieves efficiency comparable to biological quadrupeds. This work demonstrates that mechanical design choices directly enable control efficiency rather than control alone determining locomotion efficiency.

For practical research platforms balancing performance with accessibility and cost, [22] introduces the Mini Cheetah featuring custom modular actuators integrating brushless motors with internal planetary gearboxes. This design enables rapid component replacement, easy modification for experimental variations, and low-cost fabrication, making the platform accessible for accelerated research cycles. The modular philosophy proves essential for iterative design refinement.

More recently, [64] presents a chain-driven, sandwich-legged quadruped robot emphasizing reliability, safety, and cost-effectiveness. This platform employs quasi-direct-drive (QDD) actuators combining off-the-shelf BLDC motors with single-stage planetary gearboxes, achieving robust actuation without proprietary motor designs. Key innovations include robust cable strain reliefs, efficient heat sinks for thermal management, and mechanical motion limits to restrict leg motion—design features addressing practical reliability requirements often overlooked in research platforms. The dual-motor configuration reduces leg inertia while the sandwich leg architecture optimizes structural performance, resulting in a 25 kg platform developed under $8000 that successfully executes trot and crawl gaits on uneven terrain.

The mechanical design of joints fundamentally influences leg kinematics, ground reaction force control, and manufacturing complexity. [23] addresses kinematic leg design through analysis of closed-loop linkage mechanisms, examining how effective mechanical advantage changes with leg configuration and exploring optimal singularity placement. This work establishes that joint geometry design involves trade-offs between workspace, force transmission efficiency, and singularity-free regions.

Extending kinematic analysis to structural optimization, [38] develops multi-objective topology optimization frameworks for overconstrained robotic limbs, balancing competing demands for stiffness, flexibility, and mass. The resulting optimized leg designs, when fabricated through 3D

printing, demonstrate 35% improvement in obstacle clearance compared to conventional designs. This suggests that topology-optimized monolithic structures can outperform traditional articulated designs by enabling distributed compliance rather than concentrating it at discrete joints.

The evolution toward integrated compliant joint modules is exemplified by [18], which introduces novel ANYdrive compliant actuator modules combining motors, gearboxes, and electronics into single integrated units. These modules achieve torque control bandwidth exceeding 70 Hz with high disturbance rejection capability and demonstrate exceptional robustness against impulsive loads—critical for dynamic running and jumping. The integrated controller design enables real-time feedback at each joint, supporting hierarchical control architectures.

For hybrid platforms requiring rapid morphing between configurations, [66] demonstrates metamorphic aerial robot design with bi-stable arms that morph between flight and perching configurations. The use of bi-stable mechanisms enables rapid morphing in 0.97 seconds with minimal energy input, suggesting that mechanical cleverness through spring-based bistability can reduce actuation requirements in hybrid systems. This principle proves valuable for appendage repurposing in legged-aerial platforms.

In contrast to complex compliant mechanisms, [64] emphasizes simplified joint articulation using quasi-direct-drive architecture without series elastic elements, prioritizing reliability and cost-effectiveness. The sandwich-leg design integrates structural elements to maintain stiffness while reducing mass, demonstrating that simplified articulation combined with optimized leg geometry can achieve performance comparable to more complex systems.

Leg geometry profoundly affects locomotion efficiency, terrain adaptability, and achievable accelerations. The sandwich-legged architecture presented by [64] reduces leg inertia through dual-motor configuration and optimized mass distribution, enabling agile movements while maintaining structural integrity. The distributed motor placement also improves load-sharing and reduces stress concentration compared to traditional coaxial designs.

Compliant leg design offers advantages for terrain adaptation and energy efficiency. [65] develops systematic topology optimization for monolithic compliant quadruped legs, demonstrating that integrated stiffness gradients—rather than discrete rigid and compliant zones—improve both obstacle clearance and compactness. The topology-optimized designs, when fabricated through 3D printing, enable features that would be impossible or prohibitively expensive with traditional machining.

The principle of leg geometry optimization extends to gait analysis and energy efficiency. [17] provides systematic comparison of quadrupedal architectures, establishing that efficient and

versatile locomotion emerges from integrated mechanical and control design rather than actuator selection alone. Recent comparative studies extending these principles to terrain-adaptive control demonstrate that proprioceptive force feedback—whether from dedicated sensors or inferred from motor currents—enables reactive terrain adaptation without external environmental sensing.

Structural rigidity proves critical for hybrid aerial-ground platforms where torso and link flexion compromises flight stability and control precision. Component optimization through topology analysis enables achieving required stiffness targets while substantially reducing mass. [64] demonstrates that sheet metal fabrication combined with 3D printing enables cost-effective structural design, with particular attention to stress concentration at mounting locations to prevent bending under high ground reaction forces.

Weight reduction directly improves thrust-to-weight ratios essential for aerial transitions and efficient locomotion. [54] emphasizes low-inertia design principles throughout mechanical architecture, establishing that both reflected inertia (from motors and gearboxes appearing in the load) and structural inertia (mass of leg segments) must be minimized. The MIT Cheetah design achieves this through careful component selection and structural optimization.

Material selection and component consolidation strategies prove effective for mass reduction. Eliminating multi-part assemblies through print-in-place (PIP) design—such as integrating revolute joints directly into printed structures—reduces total mass while improving manufacturing simplicity and reliability. [71] demonstrates that additive manufacturing enables embedding of internal structures, integrated actuators, and optimized material gradients within single-piece components, fundamentally changing design possibilities compared to traditional subtractive manufacturing.

Additive manufacturing has transformed legged robot fabrication, enabling rapid prototyping, complex integrated structures, and cost-effective iteration. [71] presents an integrated design and fabrication strategy combining 3D printing with rapid prototyping, demonstrating unprecedented design flexibility for multi-material systems and complex geometries. The approach enables simultaneous fabrication of structural elements, mounting features, cable routing channels, and bearing pockets within single printed components.

The shift toward accessible research platforms emphasizes practical fabrication approaches. [64] adopts low-cost fabrication techniques including laser cutting and 3D printing to achieve sophisticated functionality within strict cost constraints. The combination of sheet metal components (for high-stress structural elements and efficient mass distribution) with 3D-printed structures (for complex integrated features) optimizes both cost and performance. This hybrid manufacturing ap-

proach proves more practical than monolithic additive manufacturing for large structural elements.

Custom component design directly integrated with the fabrication process exemplifies modern legged robot development. [8] develops application-driven design of 3D-printed pneumatic actuators with embedded bellows and integrated material properties, demonstrating how fabrication technology enables integrated designs. Similar principles apply to bearing-embedded motor casings and integrated cable routing channels—design features that traditional manufacturing would require as multi-part assemblies.

The benefits of rapid prototyping through additive manufacturing extend beyond speed to design flexibility. [64] emphasizes how 3D printing enables evaluation of structural robustness and mechanical failure boundaries through iterative refinement, with each iteration providing empirical data on performance and failure modes informing the next design cycle.

Integrated wire routing within structural elements improves aesthetic presentation, protects sensitive components, and eliminates external cable management complexity. Proper routing of power and signal cables within leg structures and torso components requires careful channel design to avoid interference with moving parts while maintaining structural integrity.

[75] and [67] address cable management in complex robotic systems, establishing fundamental principles of routing constraints and deformation dynamics. While these works focus on manipulating cables as primary actuators, their analysis of routing feasibility and deformation provides foundational understanding for embedding passive cable paths within robot structures.

[14] demonstrates open-source modular robot architecture principles including standardized interfaces for actuators, computing, and sensing. The architecture emphasizes clean internal organization through systematic bus arrangements and modular connectors. Custom bearing-embedded motor casing designs and leg structure channels—as implemented in [64]—facilitate seamless wire routing essential for hybrid platforms where structural integrity during high-force impacts and multi-modal transitions demands careful design.

The integration of embedded architecture with structural design proves particularly important for aerial operation. Exposed wires and loose internal components can shift during flight, affecting center of mass and control characteristics. Embedding wires directly within printed leg structures with dedicated channels enables—simultaneous achievement of structural optimization and clean internal organization.

Hybrid legged-aerial platforms represent a frontier in multi-modal robotics, requiring integration of ground and aerial capabilities without mechanical redundancy. [34] designs the Flying Star robot, demonstrating that appendage repurposing enables multimodal adaptability by combin-

ing sprawl-tuned legged crawling with aerial flight in a single integrated platform. The approach avoids dedicated appendages for each mode, reducing complexity and mass.

[32] presents the ATMO robot, achieving smooth ground-to-aerial transitions through model-predictive control adapted to near-ground aerodynamics. The work demonstrates that aerodynamic effects near ground level—often treated as disturbances—can be exploited through control to enable efficient transitions. This principle suggests that mechanical design choices enabling precise attitude control support the aerodynamic transition mechanisms.

[3] develops co-design optimization methods integrating topology, actuation, morphing strategy, and controller parameters for morphing drones. Results demonstrate 8-15% improvements in energy efficiency and mission time for co-designed drones compared to sequential design approaches, establishing that simultaneous optimization of mechanics and control yields superior hybrid platform performance.

[4] proposes passive rotary joints for rapid aerial morphing without additional actuators, achieving variable geometry in flight. This work suggests that mechanical cleverness through passive mechanisms can enable multimodal functionality without proportional increases in actuation—a critical principle for platforms where every gram impacts thrust-to-weight ratios.

The literature establishes several critical design principles directly applicable to Husky V3: Proprioceptive Actuation: Motor current-based force sensing ([72], [7]) enables high-bandwidth control without external force sensors, reducing complexity, mass, and cost. This principle supports reactive terrain adaptation and smooth aerial-ground transitions. Structural Rigidity Through Optimization: Monolithic and semi-monolithic designs using topology optimization ([38], [64]) eliminate flexion while reducing mass through informed material placement. This directly addresses the flexion problems encountered in Husky Carbon V2. Integrated Wire Routing: Embedded channel and bearing-embedded motor casing designs ([14], [64]) facilitate clean internal organization essential for hybrid platforms. Strategic placement of routing channels within printed leg structures enables simultaneous achievement of structural optimization and clean aesthetics. Simplified Articulation: Print-in-place revolute joints ([66] principles applied to ground robotics) reduce assembly complexity and component count while improving reliability through elimination of bearing installation steps and mechanical fasteners. Single-piece revolute joint designs prove more reliable than multi-part assemblies. Multi-Material Fabrication: Combined sheet metal and 3D printing ([64]) optimizes cost-effectiveness while maintaining structural performance. Sheet metal handles high-stress structural elements while 3D printing enables complex integrated features. Co-Design Philosophy: Simultaneous optimization of mechanics and control ([3], [32]) yields superior hybrid

platform performance compared to sequential design. Mechanical choices should be informed by anticipated control strategies rather than designed independently. Dual-Motor Leg Architecture: The sandwich-leg configuration ([64]) reduces leg inertia, improves load distribution, and enables simplified joint design compared to coaxial architectures. Distributed motor placement also improves structural efficiency.

Chapter 3

Methodology

3.1 Methodology Overview

The development of Husky V3's with much robust hardware and smooth multi-modal capabilities necessitated a comprehensive initial design review to assess mechanical feasibility, identify structural deficiencies, and establish design refinement priorities. The design review process was systematized across three hierarchical levels: (1) general leg architecture common to all four limbs, (2) leg-specific assemblies (Legs 1-4), and (3) torso. Following identification of design deficiencies, an iterative redesign process was implemented, progressing through component-level refinements, mechanical subassembly integration, electrical routing, full leg assembly, torso integration, and final system assembly

3.2 Initial Design Review Protocol

A structural inspection was conducted on the assembled Husky V2 refer Fig. 3.1 to evaluate mechanical performance, component integration, and bearing/fastening integrity across all major subsystems. Observations were categorized by assembly hierarchy and documented to inform iterative design modifications.

3.2.1 General Leg Architecture Review

Inspection of the common leg design revealed six primary design considerations requiring modification:

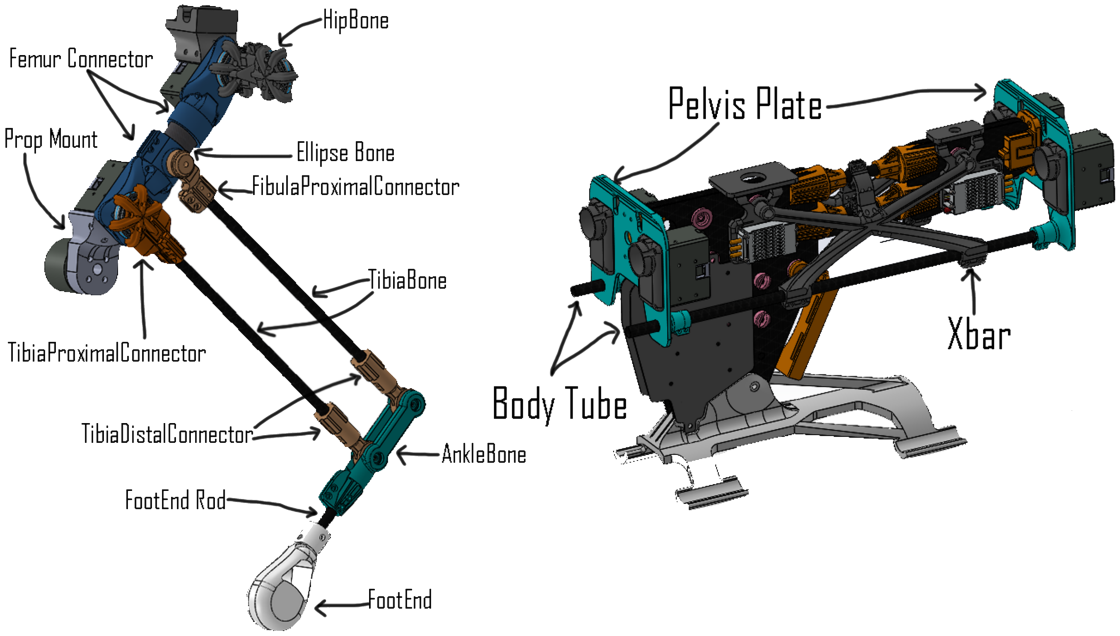

Figure 3.1: Shows leg assembly of Husky V2

Fastening and Connector Design:

- Clamp designs in femur connectors exhibited inadequate clamping force distribution, necessitating geometric redesign for improved load transfer
- Tibia connectors were over-constrained at both ends. Removing the end clamps reduced parasitic stiffness and enhanced compliance
- Foot-end clamping mechanisms required redesign to accommodate proper fastener engagement and load distribution

Passive Compliance Architecture: The fibula proximal connector (passive element) exhibited elastic behavior under compression and demonstrated undesired contact against the femur connector during load conditions, indicating the need for geometric refinement to maintain separation and proper compliance characteristics

Fastener Standardization: Hip bone fasteners lacked uniformity across the four legs; standardization of screw specifications (length, diameter, material) was prioritized to reduce component inventory and ensure consistent mechanical properties

Optional Weight Optimization: Propeller mounting and flight lock architecture were identified as candidates for lightweight redesign

3.2.2 Leg-Specific Assembly Review

Individual inspection of each leg revealed localized design and assembly deficiencies:

Leg 1 (Front Right):

- Fibula proximal connector exhibited excessive play (wobbling) primarily attributable to bearing assembly clearances exceeding design tolerances
- Knee motor (FRK-11) demonstrated increased stiffness and potential mechanical damage compared to identical units in remaining legs, suggesting a manufacturing defect or improper assembly
- Knee claw connector required re-fabrication with proper fastener specifications

Leg 2 (Back Left):

- Hip bone assembly identified as requiring re-fabrication due to fastener specification errors (screw length and quantity)
- Tibia bone exhibited anomalous acoustic emissions and rotational drift, indicating internal structural damage or component degradation
- Tibia distal connector demonstrated mechanical failure requiring replacement

Leg 3 (Front Left):

- All fasteners and design elements, with the exception of general leg architecture items, met design specifications and required no immediate modifications

Leg 4 (Back Right):

- Tibia bone assembly generated significant acoustic noise during manual articulation, consistent with internal bearing or fastening degradation
- Hip bone assembly exhibited fastener specification errors identical to Leg 2, requiring standardized re-fabrication

3.2.3 Torso System Review

Inspection of torso-mounted subsystems revealed structural and integration issues:

Electrical Power Architecture: Voltage regulator mounting plate exhibited a mechanical fracture, necessitating redesign to accommodate thermal expansion cycling and vibration isolation

Structural Integration:

- Front plate torso mounting assembly revealed two missing fastener nuts, indicating incomplete assembly or loss of components during handling
- Anti-twist cross member (lateral stiffening element) exhibited inadequate torsional rigidity and improper load distribution, requiring geometric modification and reinforcement
- Battery mounting interface lacked sufficient mechanical stability; redesigned mounting brackets were required to prevent battery shifting during dynamic locomotion

General Mechanical Wear: Plate clamps around torso-mounted rods demonstrated accelerated wear patterns, suggesting either inadequate material selection, improper preload specification, or manufacturing surface finish defects

3.3 Design Evolution and Refinement

3.3.1 Torso Structural Integrity

The original torso structure as shown in Fig.3.2 suffered from three critical design flaws that compromised structural integrity during operation. Motors mounted directly on a thin pelvis plate caused inward lean of motor assemblies, while hip motor torque loads transmitted through flexible structures induced body twist and misalignment. Additionally, body tube clamps positioned at far end corners created uneven load distribution and caused parallel slipping under operational loads. To address these issues, the refined design integrated several key structural improvements: body tubes were enveloped directly into the pelvis plate structure for symmetric load transfer centered at motor positions, dual-contact body tube mounts supported by reinforcing ribs were implemented to resist roll and yaw loads more effectively, pitch resistance was achieved through upper

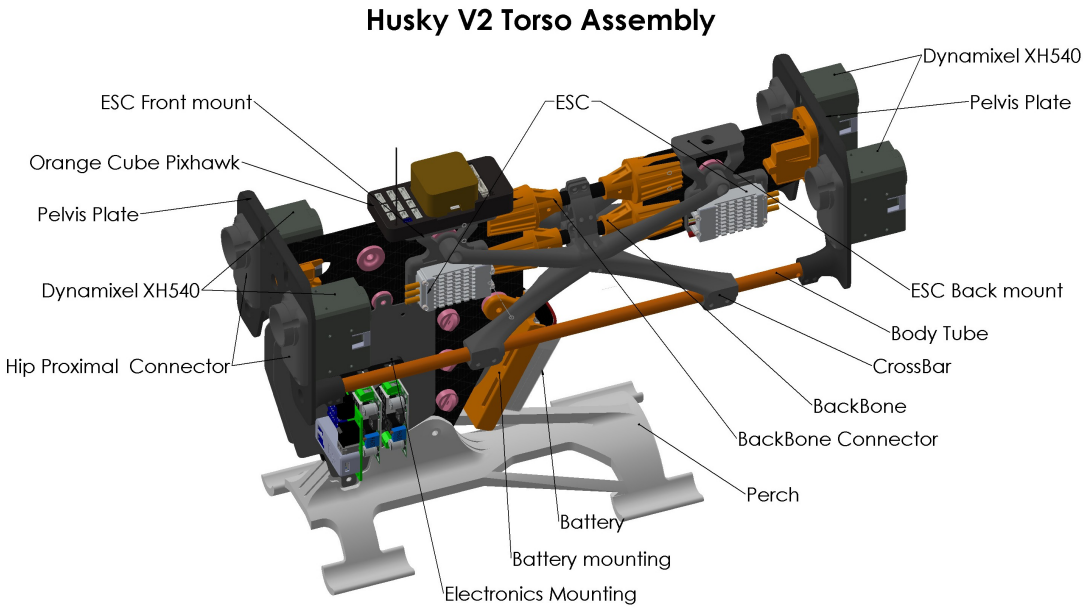

Figure 3.2: Shows the Husky V2 torso with electronics having Jetson Nano on one side and Voltage regulator and U2D2 board on the other.

and lower body tube enclosures creating a fully-constrained structural frame, and the cross member was converted from a floating design to direct plate-to-plate fastening to establish continuous torsional load paths throughout the structure.

Initial prototype testing of the ribbed pelvis plate seen in Fig.3.3 revealed four primary fabrication and assembly challenges that required iterative refinement.

- **Support Structure Fragility:** Delicate support structures for dual-contact body tube mounts broke during support material removal; resolved by reorienting the part for upward-facing rod printing to reduce support complexity.
- **Insufficient Clearance for Hip-Bone Rotation:** Limited clearance during aerial-to-legged mode transformation constrained joint articulation; clearance geometry around the pelvis articulation zone was increased to accommodate full range of motion.
- **Lower Backbone Mounting Conflict:** Backbone mounting interface clashed with ridge structure, restricting torso movement; ridge geometry was repositioned to provide adequate clearance for torso articulation during mode transitions.

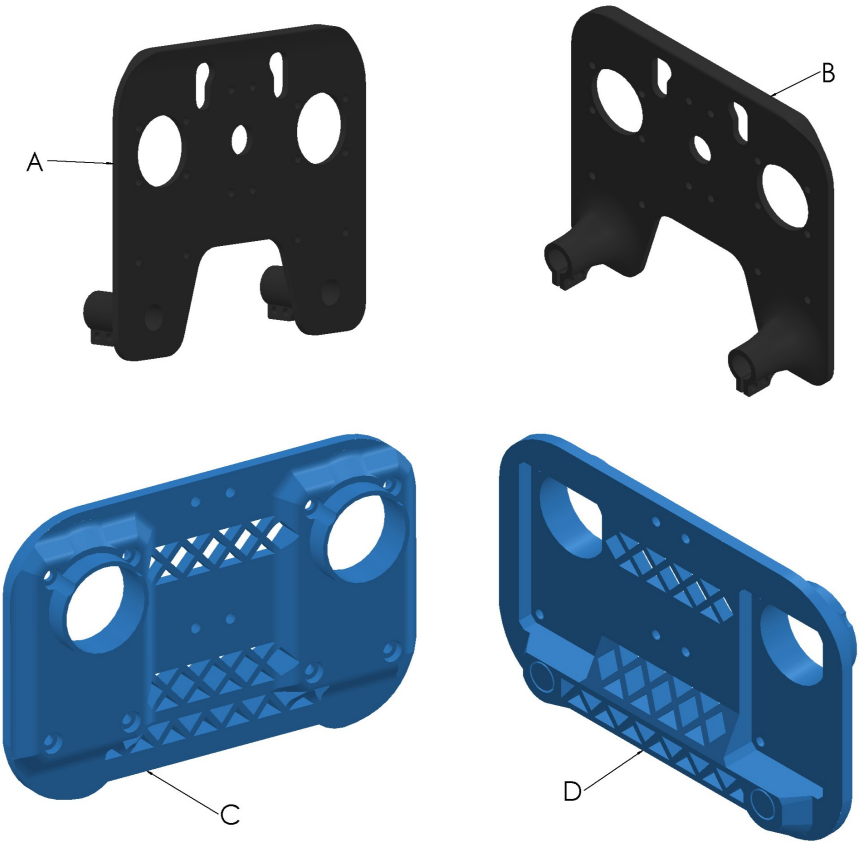

Figure 3.3: Shows comparison of old and initial iteration of redesign for Pelvis Plate. (A) & (B) are isometric views of Old Pelvis Plate, (C) & (D) are the isometric view of initial redesign.

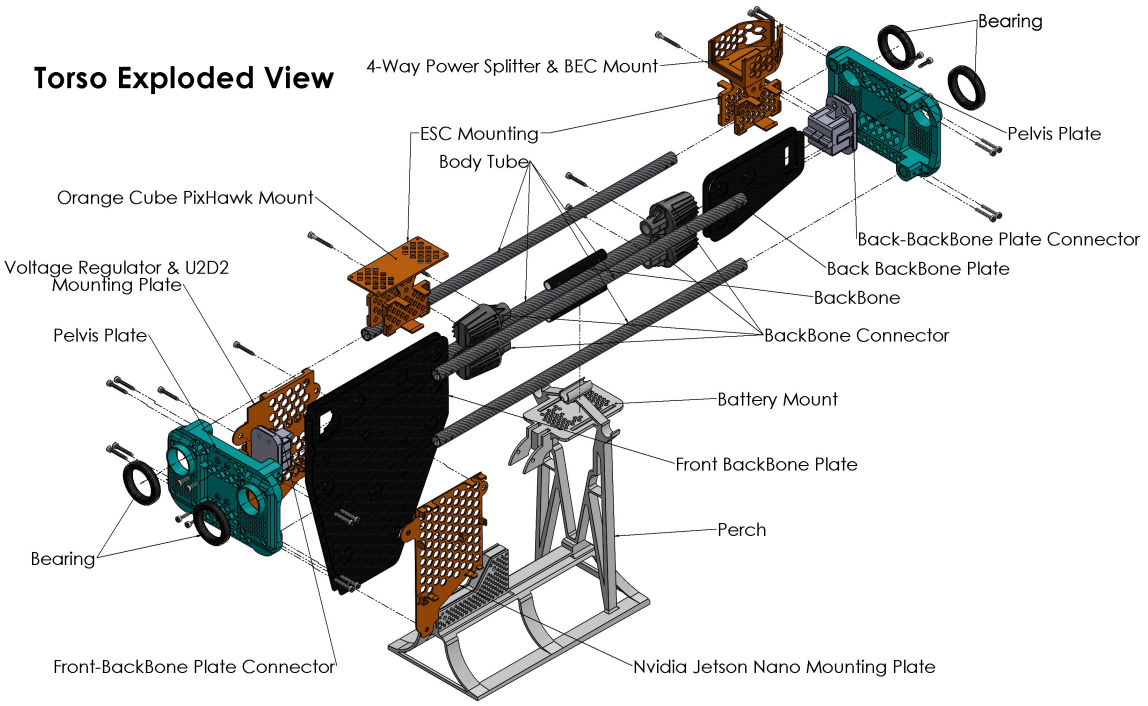

Figure 3.4: Exploded view of the new Torso

- **Inadequate Screw Mounting Distance:** Screw mounting distances from base proved insufficient for proper fastener engagement and load transfer; base offset distance was increased to ensure reliable fastener seating and secure attachment of carbon fiber rods.

To address torso twist issues, the design was further refined by incorporating two additional carbon fiber rods for enhanced flex resistance. To mitigate the resulting weight increase, a larger-diameter carbon fiber rod was selected with reduced wall thickness: 1 mm thickness with 12 mm outer diameter and 10 mm inner diameter, compared to the previous 2 mm thickness with 10 mm outer diameter and 6 mm inner diameter. The larger diameter provided proportional structural strength while maintaining reduced mass. These rods were enclosed using a dual-contact grip design that secured the carbon fiber rod from both internal and external surfaces, providing firm constraint and preventing slippage. This integrated approach yielded a robust torso structure that effectively resisted torsional flexure while maintaining mass efficiency objectives. Figure 3.4 illustrates the final ribbed pelvis plate design, demonstrating significantly improved torsional rigidity compared to the previous iteration while preserving controlled flexibility.

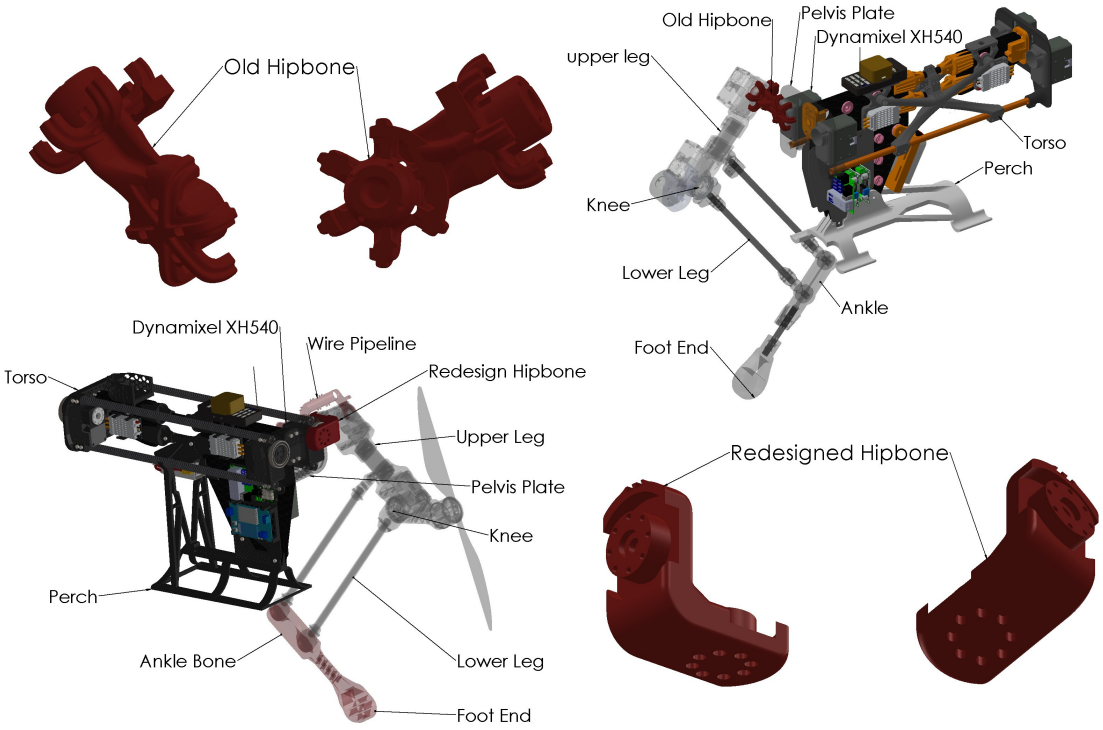

Figure 3.5: (A) & (B) are isometric views of Old HipBone, (C) & (D) are the isometric view of New Hipbone Design

3.3.2 Hip Bone Redesign

The original hip bone refer Fig.3.5 exhibited three critical deficiencies that compromised assembly quality and structural performance. Motor mounting screws positioned in-line with perpendicular motor mount features created severe accessibility constraints, preventing adequate fastener torquing and integrity verification. The original claw design for bearing capture demonstrated inadequate grip strength and flexure under load, causing loss of bearing preload and increased runout during dynamic operation. Additionally, the extended stem length created excessive moment arm for motor mounting, amplifying torque reaction loads on the femur connector and increasing structural deflection proportionally with load, which degraded motor positioning accuracy. To address these issues, an iterative design evolution was pursued: the first iteration introduced an L-shaped Y-grip design with internal rib structures for distributed load bearing and repositioned fastener axes to improve motor screw accessibility, successfully shortening the stem to reduce moment arm. However, printing complexity remained high. The final design adopted an L-shaped C-grip configuration

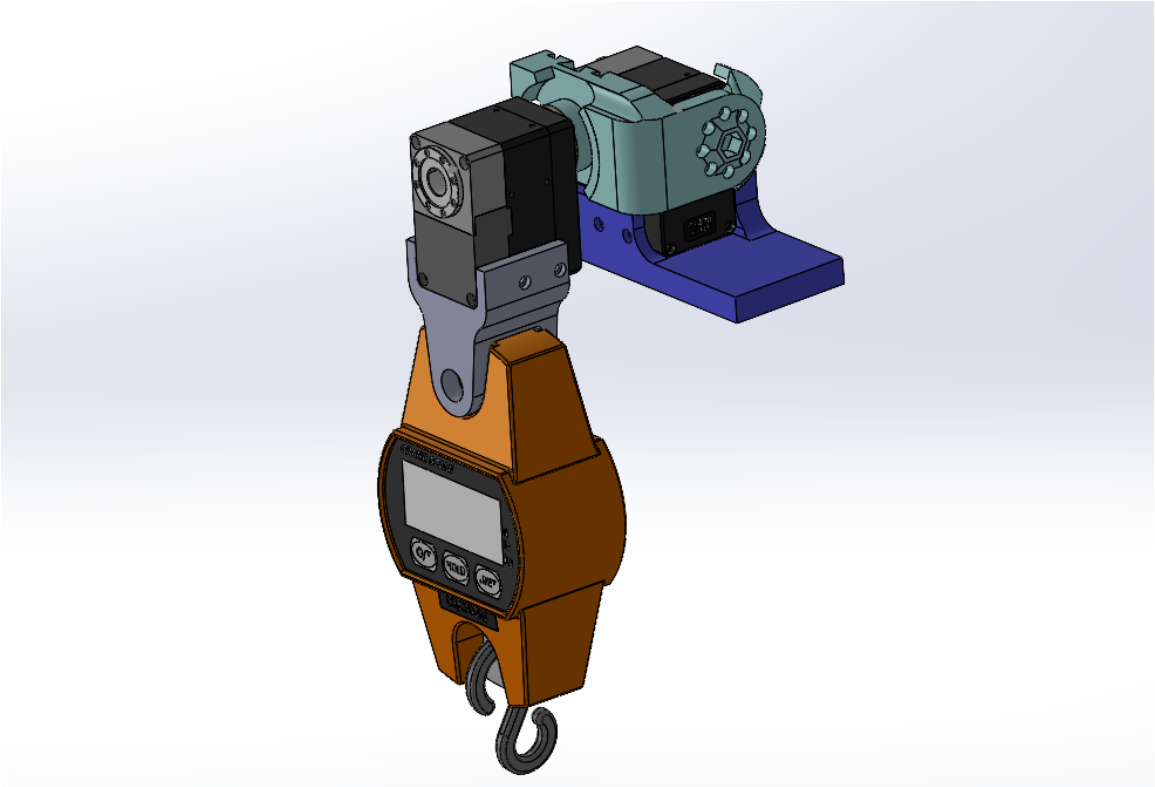

Figure 3.6: shows the setup for testing the Hipbone with toque enabled motor.

that simplified claw geometry for improved 3D printability while maintaining accessibility for both motor-mounted fasteners, achieving a 7-gram weight reduction and improved bearing grip through optimized contact geometry.

The final L-shaped C-grip hip bone design integrated several key improvements to resolve identified deficiencies. Optimized claw geometry provided positive bearing restraint with reduced material, while dual motor fastener accessibility was achieved through independent screw paths that avoided geometric conflicts. Integrated internal ribs distributed loads effectively without excessive material addition. These refinements collectively enhanced assembly accessibility, bearing retention reliability, and structural load path efficiency, validating the transition from the original constrained design to a more functional and fabrication-friendly design.

Load Testing Validation: Tensile strength testing of the hip connector was conducted using the following experimental protocol as shown in Fig.3.6. A blue mounting bracket was fastened to the test table to establish a fixed reference point, and a motor assembly was installed on the hip bone.

Incremental loads were applied in 2.6 kg intervals ranging from 0.5 kg to 10 kg, with simultaneous measurement of motor position error and motor current consumption(calibrated at 0.088°/value and 2.69 mA/value, respectively, based on the Dynamixel Datasheet). This methodology enabled quantitative assessment of structural deflection and motor performance degradation under progressively increasing load.

Stage	**Load Range (kg)**	**Deflection (°)**	**Current (mA)**
L1	0.5–3.1	0.44	270
L2	3.1–5.7	0.53	242
L3	5.7–8.3	0.88	470
L4	8.3–10	0.53	269
Total	0.5–10	2.38	1,520

Table 3.1: Deflection and current measurements across different load ranges

From Table 3.1, the hip connector demonstrated linear load response up to 10kg, validating the redesigned geometry for Husky V3's operational loading envelope.

3.3.3 Hip Distal Connector Redesign

The original Hip Distal connector exhibited insufficient clamping geometry as seen in Fig.3.7, resulting in femur-bone slippage under dynamic loads and inadequate bearing capture with preload loss. Iterative refinement focused on three areas: optimized bearing grip surface geometry for enhanced contact and restraint, increased structural depth for improved bending resistance, and simplified clamping action for improved assembly reliability. The final redesigned femur connector achieved enhanced clamping geometry with optimized bearing contact surfaces and improved structural stiffness, ensuring positive femur restraint and reliable bearing preload maintenance during operation.

Load Testing Validation: Femur connector tensile strength testing established a critical manufacturing principle: parts oriented with load direction aligned to the Z-axis printing direction demonstrate maximum tensile strength, indicating that optimal fabrication orientation significantly enhances structural performance. Validation testing compared two specimens fabricated with different printing orientations, revealing a key finding in robustness: despite orientation variations, both specimens withstood loads of approximately 18 kgf or greater. This result in fig.3.8 demonstrates

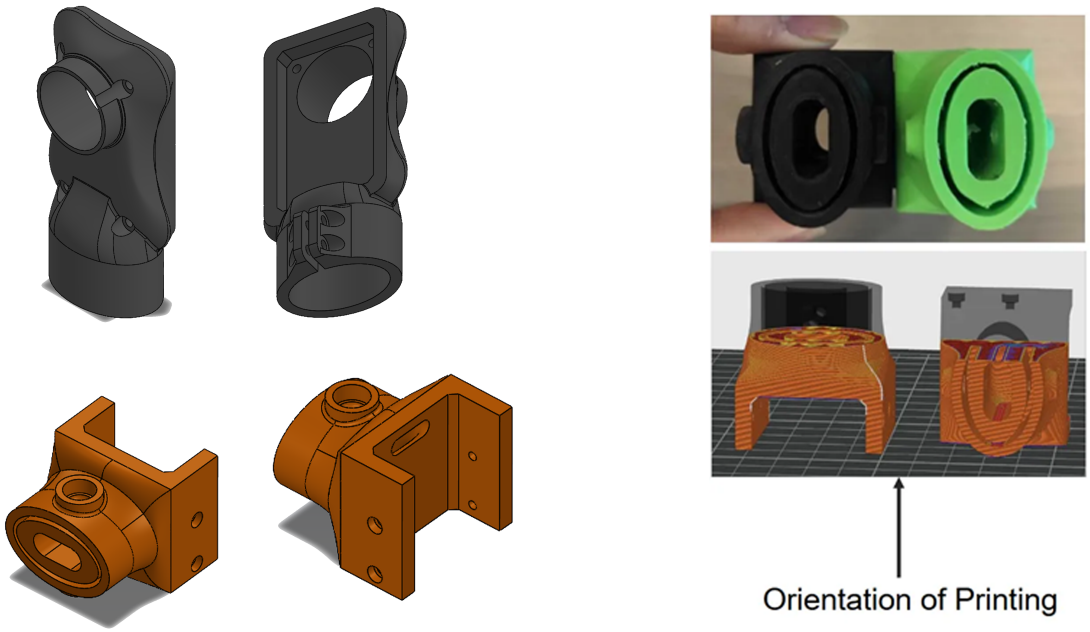

Figure 3.7: shows comparison of the old and new HipDistal Connector, and the image on the right shows the printing orientation and under test, both orientations demonstrate similar load-bearing results.

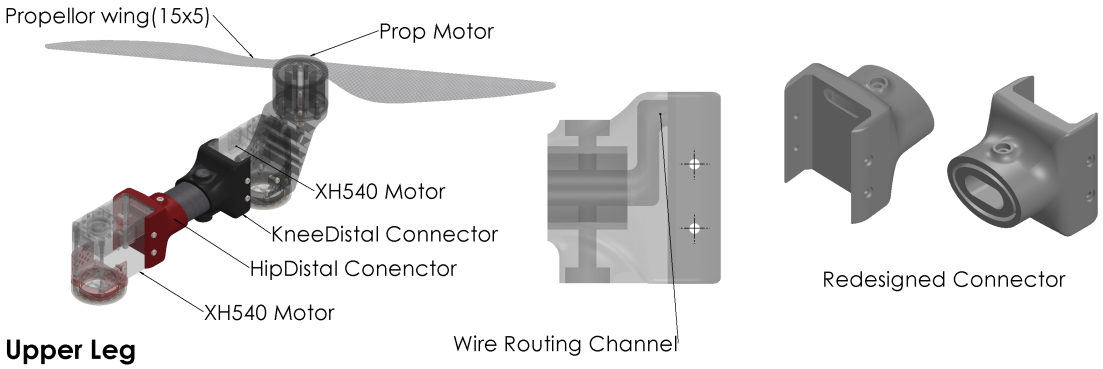

Figure 3.8: Shows the redesigned HipDistal Connector and the wire routing channel.

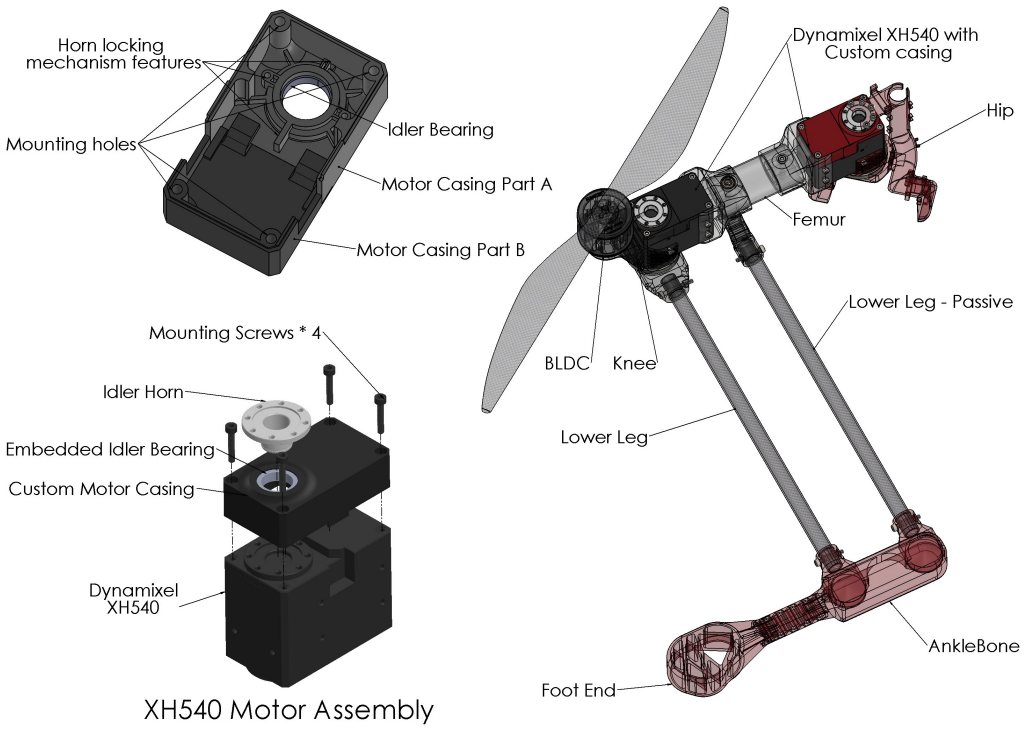

Figure 3.9: left bottom shows the exploded view of the XH540 motor assembly, left top figure represents the motor casing with embedded bearing, and right figure is a reference for the locations of this motor assembly.

that the redesigned femur connector maintains structural reliability independent of fabrication orientation, providing manufacturing flexibility without sacrificing performance. The redesigned femur connector successfully achieved reliable femur link restraint across all operational loading conditions, with demonstrated load capacity exceeding 18 kgf. This design robustness across multiple printing orientations validates both the structural refinement and the practical fabrication of the component for field deployment.

3.3.4 Motor Casing with Idler Support

The primary objectives for motor casing design, shown in fig.3.9, were establishing clean wire routing for thick 16-gauge wires and providing firm passive side support for the idler pulley system. The design underwent iterative refinement to address multiple challenges. The implementation of idler horn locking was based on dynamixel mechanisms, and reusing peripheral dynamixel

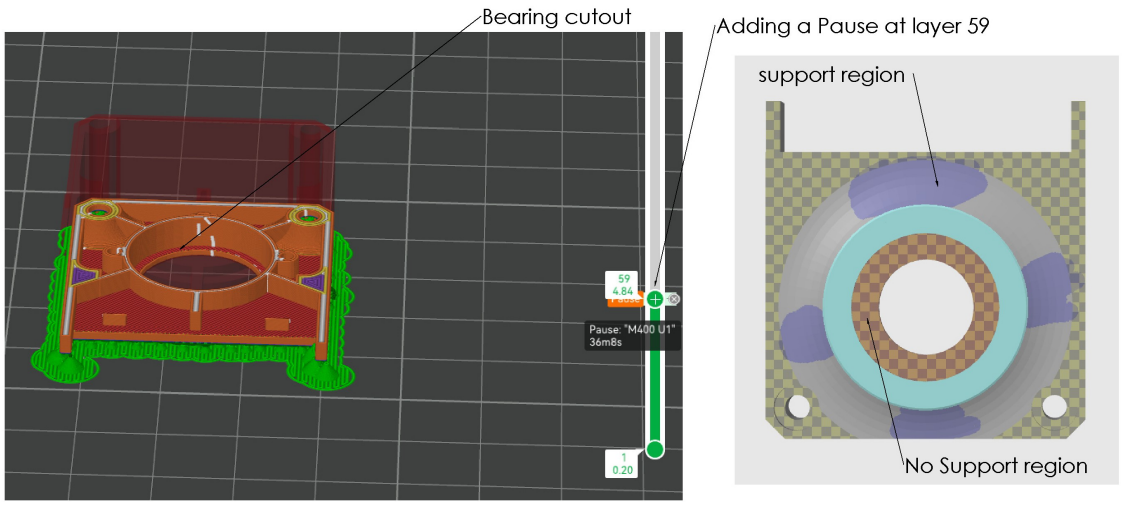

Figure 3.10: left image shows the slicing interface of adding a pause, and the right image shows support painting

parts required careful geometric adaptation. Achieving precise tolerances for press-fit bearing installation while securing the plastic clevis clip proved particularly challenging. Once these initial challenges were resolved and the casing was mounted, dynamic leg flexure during operation caused bearing displacement and idler horn detachment from the casing. To address this issue, a bearing embedding strategy was implemented: the 3D printing process was paused at a critical stage, and a bearing was manually inserted into a predesigned cutout, ensuring secure bearing retention during subsequent dynamic loading. This hybrid fabrication approach successfully eliminated bearing slippage and maintained idler horn stability throughout operational cycles. The bearing embedding methodology is demonstrated in Fig. 3.10 and is executed through the following procedure:

1. Design the Cutout
2. Create a cutout in your design that encompasses the bearing's dimensions.
3. **Slice the Model:** slice the model in Bambu Studio and scroll through the layers to review your design.
4. **Check for Supports:** verify that no supports are present in the embedding region. Removing supports while the print is paused can shift the bearing, causing print failure.

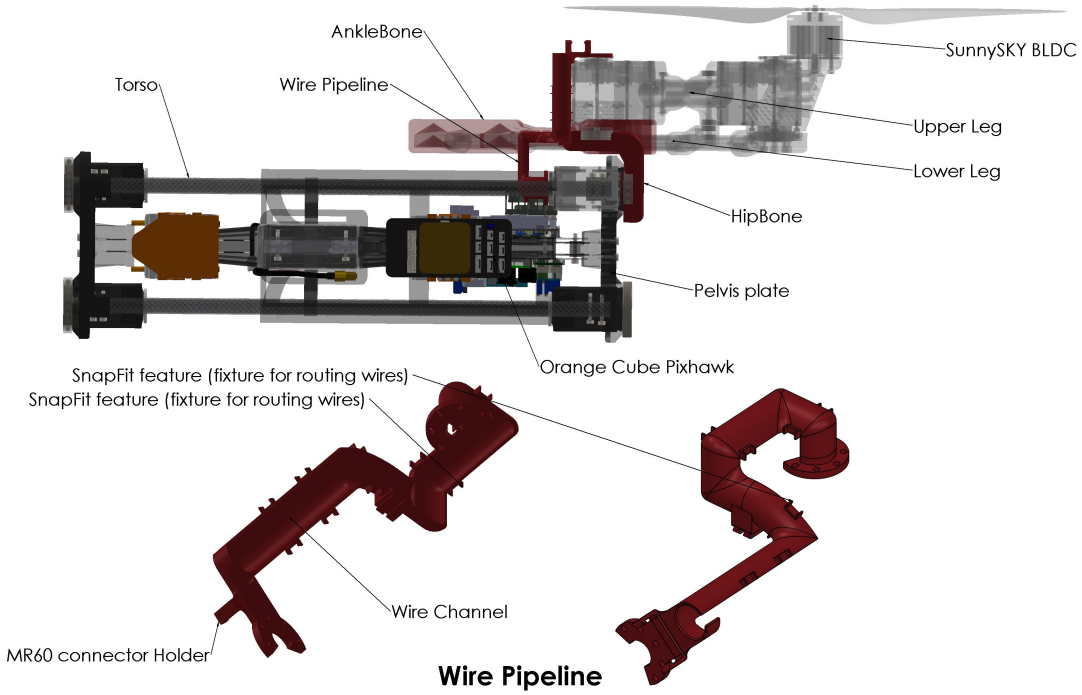

Figure 3.11: Translucent view of the front left upper leg to observe the wire routing path(orange wire)

5. **Remove Unwanted Supports (if needed):** If supports appear in the embedding region, use the support painting tool in Bambu Lab. Right-click to paint the regions where supports should not generate.
6. **Slice Again:** slice the model again after removing the unwanted supports.
7. **Add a Pause Command:** add a pause command right before the interfacing layer begins at layer 59 or 4.84 mm height from the bed.
8. **Insert the Bearing:** When the print pauses, insert the bearing into the cutout.

Resume the print and watch a few layers to confirm the embedding is successful and the bearing remains properly positioned.

3.3.5 Wire pipeline

Once the wire exits the motor casing of the hip sagittal motor, it must route through the passive side and into the rear of the hip frontal motor. To achieve clean, organized wire routing

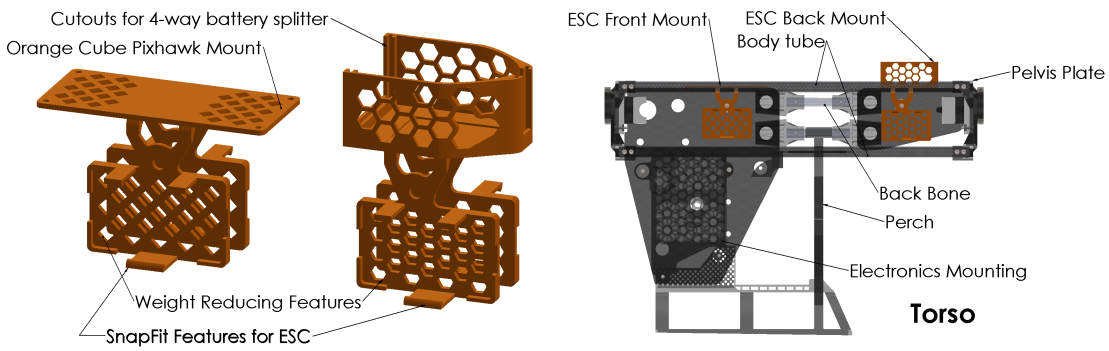

Figure 3.12: Translucent view of the front left upper leg to observe the wire routing path(orange wire)

in this critical transition zone, a specialized wire guide design was developed. This component secures the wires while enabling tangle-free motion and preventing interference with motor operation. The wire guide design ensures proper cable management throughout the dynamic range of motion, maintaining structural organization and protecting against potential entanglement during terrestrial and aerial mode transitions. The design and use can be seen in Fig. 3.11 and 3.20.

3.3.6 Electronic Speed Controller (ESC) Mounting

ESC mounting brackets were redesigned to address excessive weight, bulky features, and poor thermal management. Snap-fit assembly and lightweight geometry reduced system mass, while improved thermal pathways and enhanced EMI shielding improved component reliability and heat dissipation during sustained operations. The features and snap fit design can be observed in the fig.3.12.

3.3.7 Ankle Bone - Living Hinge Articulation

Iterative development introduced elastomeric elements for distributed compliance and systematically evaluated multiple living hinge geometries. Initial prototypes refer to A, B, D, and E in Fig.3.13 exhibited three primary issues: excessive slack in the articulation system, elevated friction during joint rotation, or unfavorable printing orientations that resulted in structurally weak components. Following comprehensive testing, design C in fig.3.13, a conical geometry design, demonstrated promising performance characteristics.

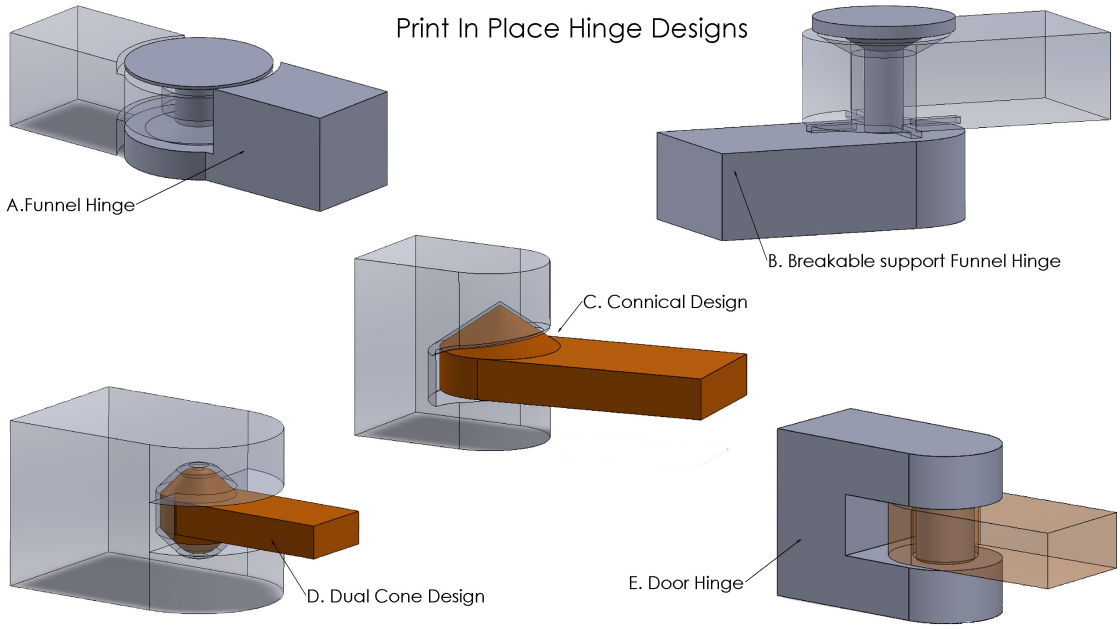

Figure 3.13: Shows PIP living Hinge design concepts for the ankle joint.

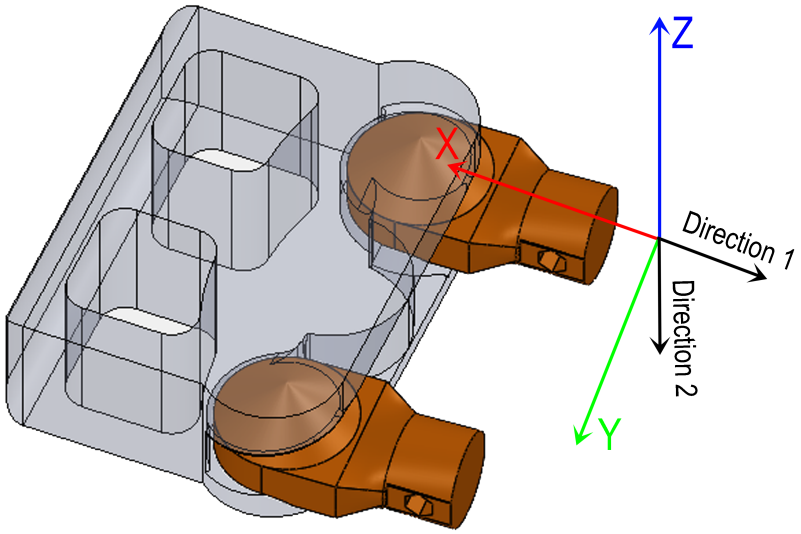

Figure 3.14: displays the directions of load that could act on the joint under the dynamic motion of the robot.

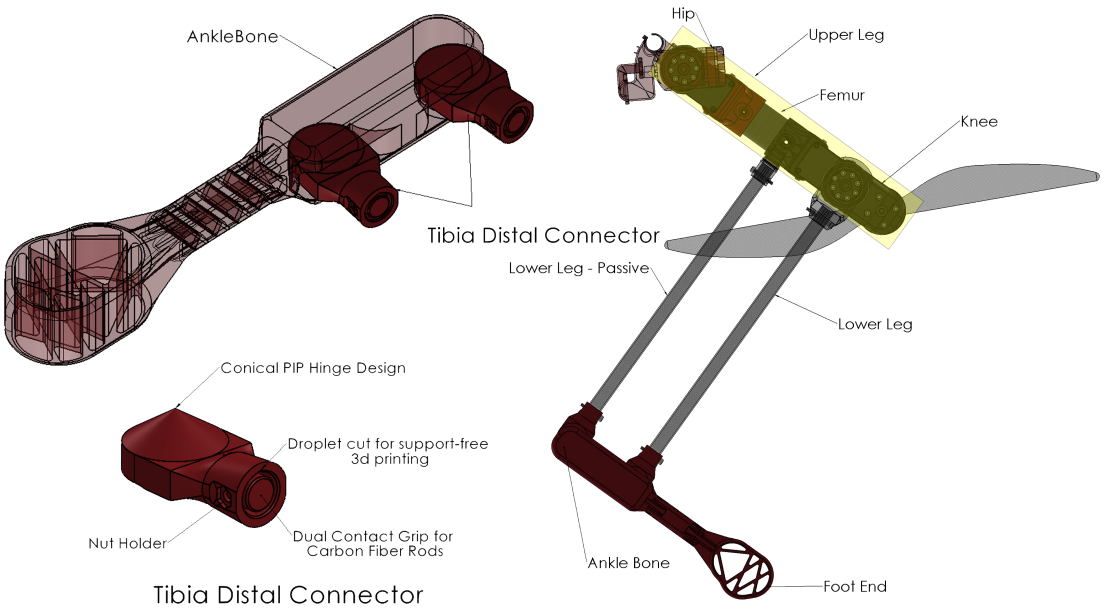

Figure 3.15: Redesign Ankle bone wireframe view, TibiaDistal Connector and Leg Orientation.

This refined design leveraged an innovative Print In Place (PIP) fabrication approach, eliminating post-print assembly requirements. The living hinge features a conical geometry with 33-degree slopes optimized to exploit the 3D printer's overhang printing capability, enabling direct fabrication of a fully functional PIP articulated joint. This design methodology combined advanced geometry optimization with additive manufacturing process capabilities, substantially reducing assembly complexity and improving manufacturing efficiency. Fig.3.14 shows load testing direction for validating this design approach: Direction 1 achieved approximately 25 kg load capacity without breakage, while Direction 2 recorded approximately 23 kg, demonstrating robust performance across multiple loading orientations. The parallel arrangement of the two revolute joints enables load sharing and prevents concentrated stress, enhancing the overall torsional stiffness and reliability of the articulated ankle system. Simulated ground contact loading tests further confirmed ankle bone living hinge performance by characterizing hinge deflection across the operational load range, demonstrating repeatability over multiple loading cycles, and verifying compliance property retention without permanent deformation. These validation results establish design reliability for field deployment, shown in Fig.3.15.

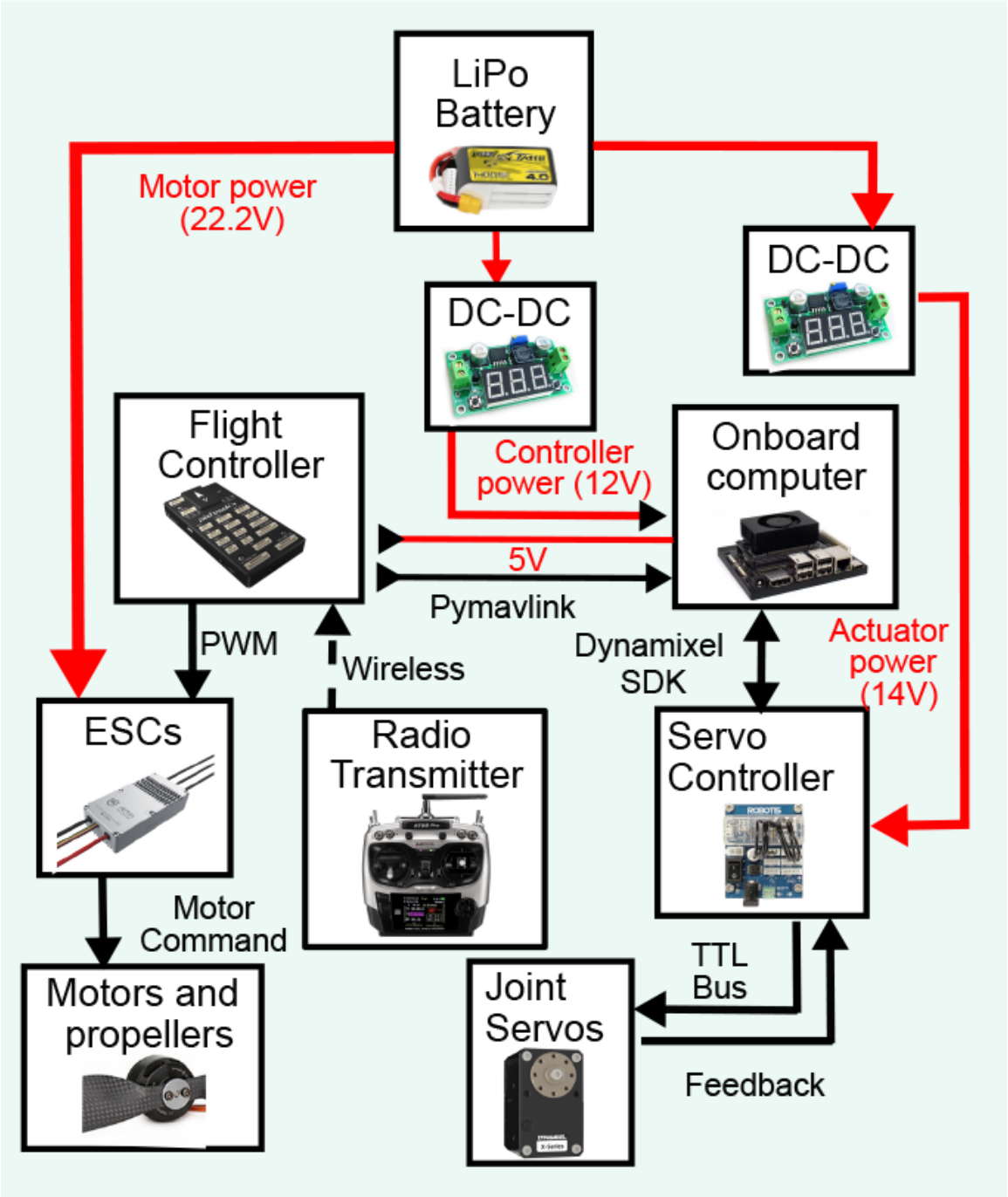

Figure 3.16: show the signal and power architecture of Husky V3 which is the same as Husky V2. Image: Chenghao Wang

3.3.8 Electronics Architecture

The Husky V3 platform employs the same electronics architecture as Husky V2 as seen in Fig.3.16. A 22.2V LiPo battery serves as the primary power source, feeding two DC-DC converters that regulate voltage to 12V for controller systems and 5V for onboard computing subsystems. Motor actuation is powered directly at 22.2V through Electronic Speed Controllers (ESCs), which receive PWM commands from the flight controller and drive the four brushless motors and propellers for aerial propulsion. The central Pixhawk flight controller manages aerial dynamics and coordinates PWM outputs to the ESC array while receiving wireless commands via radio transmitter and pymavlink protocol. Legged locomotion is controlled through a Jetson Nano onboard computer operating at 12V, which communicates with the servo motor controller via the Dynamixel SDK protocol. The servo controller manages all twelve joint servos through a TTL bus network, providing coordinated leg motion and receiving feedback for real-time kinematic adjustments. All components operate in synchronized harmony through multiple communication protocols—Pymavlink for flight control, Dynamixel SDK for actuator coordination, and wireless radio telemetry for external command input—enabling seamless transitions between terrestrial and aerial locomotion modes while maintaining centralized power distribution and decentralized functional control architecture.

3.4 Assemblies

This section covers the details on how the assemblies are designed starting with torso, Upper Leg, wire routing and finally ending with lower leg and ankle .

3.4.1 Torso Assembly

Torso assembly is relatively straightforward, as illustrated in Figure 3.17 and Figure3.18. Four carbon fiber body tube rods, each 395 mm in length, are attached to the pelvis plate and secured with screws. In parallel, the backbone assembly is prepared. This backbone design is inherited from the Husky family architecture: front and back plates are embedded in the backbone plate connector and backbone connector, which are then assembled with the carbon fiber backbone rod. The front backbone plate connector is screwed into the assembled pelvis plate, and a second pelvis plate is attached from the rear, fully enclosing the backbone assembly. Following this step, the motors, ESC mounts, electronics mounts, and perch are installed. Finally, the voltage regulator, U2D2 board, and BEC (Battery Elimination Circuit) are mounted as shown in Figure 3.16. 3.17.

Figure 3.17: Shows the new assembled torso with electronics having Jetson Nano on one side and Voltage regulator and U2D2 board on the other.

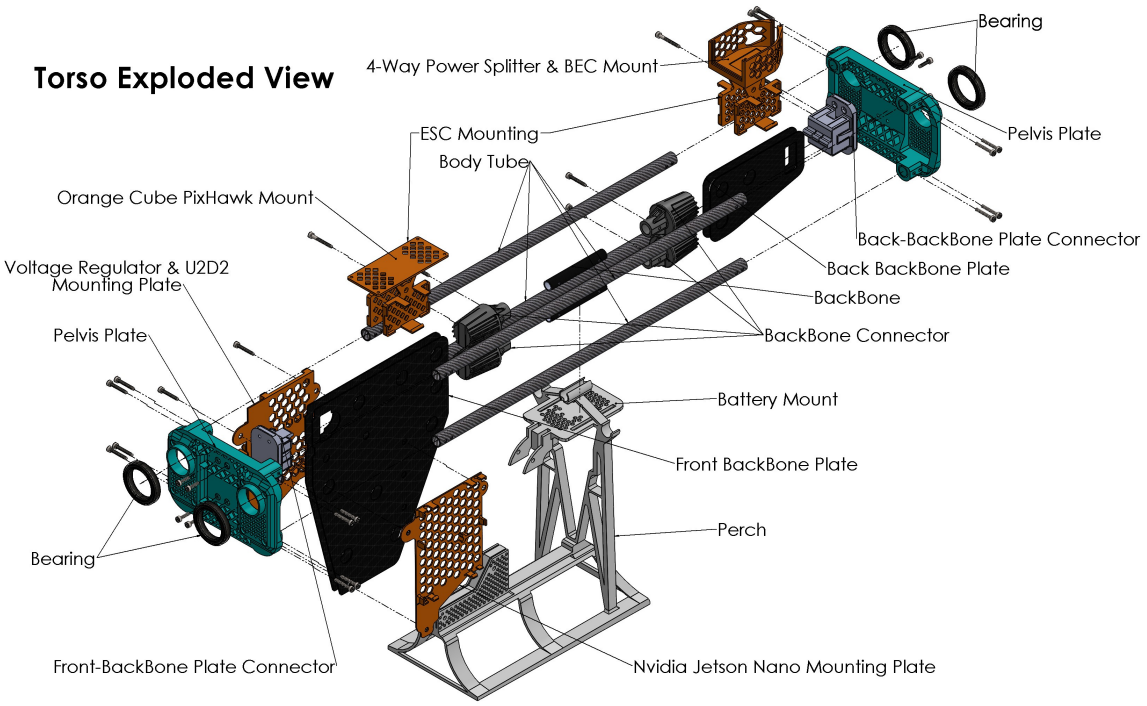

Figure 3.18: Shows the exploded view of new assembled torso without electronics.

3.4.2 Upper Leg Assembly

In Fig. 3.19, assembly of this integrated system begins at the BLDC motor end, where the motor is mounted on the knee proximal connector. Wires are then routed through the motor casing and exit directly into the knee distal connector. Managing the passage of three 16-gauge wires and three 22-gauge wires through the confined channel requires a systematic assembly procedure. The 22-gauge wires are routed first, followed by using a single-strand wire as a guide to thread the thicker 16-gauge wires through the channel and out toward the femur. Before inserting the femur into the connector, a small washer is placed through the knee distal connector's hole. This washer protects against potential damage during femur screw fastening and interlocking. A similar assembly sequence is repeated for wire routing through the hip distal connector into the hip sagittal motor casing, with wires exiting through the idler horn. This methodical routing strategy ensures proper wire organization while protecting conductors from damage during assembly and operation.

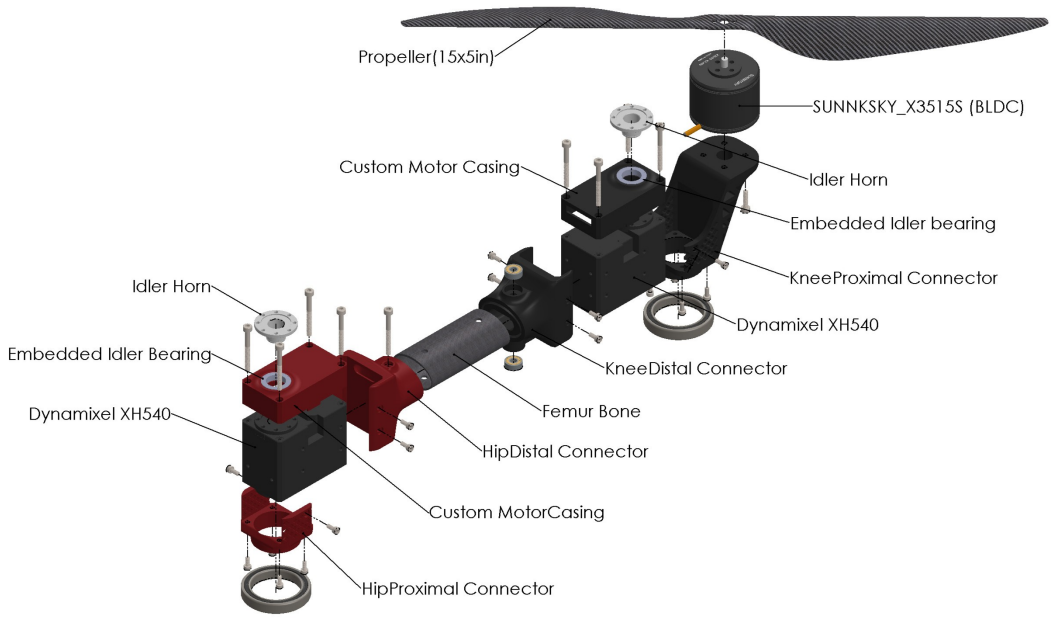

Figure 3.19: Shows the exploded view of the Upper Leg Assembly.

3.4.3 Wire Routing

The routing of wires represents a critical design consideration for operational safety and system reliability. Proper cable management protects the robot from two primary hazards: entanglement in the radial line of motion of sagittal motors and potential damage from propeller blade contact. Beyond safety considerations, effective wire routing provides significant cosmetic advantages, contributing to a clean and professional appearance of the Husky v3.

The wire routing system begins at the knee BLDC motor with three 16-gauge wires. These wires travel through the motor casing internally, then continue along with the dynamixel communication wires through the designed channels in the knee distal connector to the hip sagittal motor. From there, the wires exit and travel parallel to the sagittal motor through a dedicated routing pipeline. The cables enter the hip frontal motor's passive side and exit on the opposite side, where the daisy-chained dynamixel motor cables connect to the splitter board via the U2D2 interface. Separately, the BLDC wires connect directly to the ESC (Electronic Speed Controller). Fig.3.20 gives a visual of the wire path through the parts.

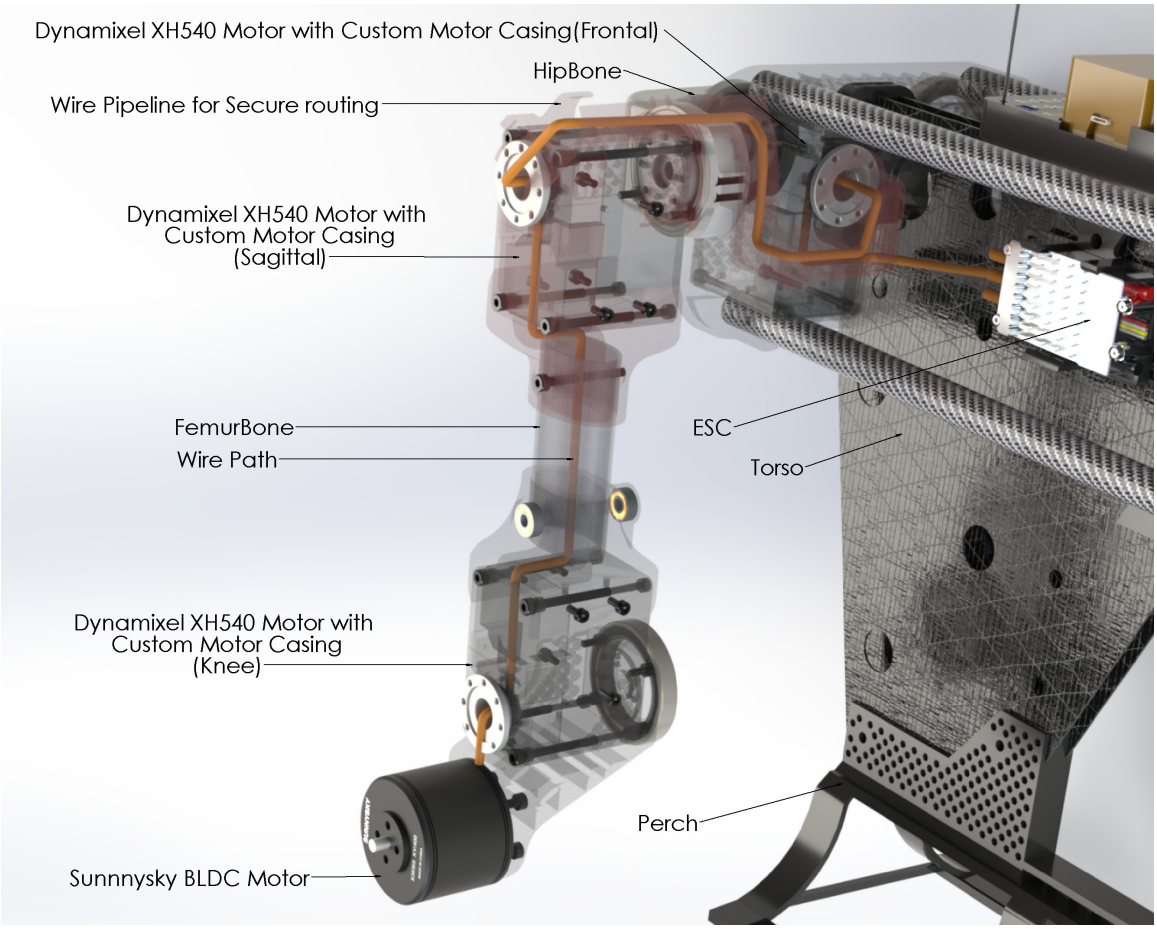

Figure 3.20: Translucent view of the front left upper leg to observe the wire routing path(orange wire)

Figure 3.21

3.4.4 Lower Leg & Ankle Assembly

From a kinematic standpoint, the lower leg and ankle represent two distinct links with separate functional roles. The Tibia Proximal connector functions as part of the lower leg link, while the ankle assembly operates as an independent articulated joint. Due to the PIP fabrication approach, the Tibia Proximal connector is printed as an integrated component of the ankle bone and cannot be separated without damage. The ankle bone printing orientation is critical: the part is positioned flat on its side with the cone joint tip facing upward. Crucially, the cone tip must be oriented perpendicular to the print bed to ensure proper geometry and structural integrity. A Droplet design feature, previously detailed in Fig.3.15, is incorporated to facilitate tibia bone insertion into its connector. Since the ankle assembly is fabricated as a complete unit, no post-print assembly is required. The Fibula Proximal connector features two 4x11x4 bearings positioned on opposite sides to enable smooth passive rotation and is secured to the knee distal connector using a shaft screw through the designated through-hole location, as shown in Fig.3.21.

Chapter 4

Results

This chapter presents the validation process for Husky V3, focusing on the innovative print-in-place (PIP) articulated joint and optimized lightweight design. Testing procedures evaluate structural integrity of refined components including the pelvis plate, hip bone, femur connector, ankle living hinge, and ESC mounting brackets. Experimental protocols assess load capacity, compliance retention, and durability across operational conditions. Wire routing integration is documented for both functional performance and aesthetic presentation. Validation confirms Husky V3's structural reliability and component performance under dynamic operational loading.

4.1 Prototype Overview

A primary design objective for Husky V3 was the elimination of torso and leg flexion, which had significantly compromised walking gait stability and flight control in previous iterations. The prototype maintained the original kinematic architecture without scaling factors, preserving the fundamental locomotion principles established in earlier designs. A notable design modification repositioned all hip frontal motors internally within the torso structure, departing from the previous external mounting configuration. Despite this geometric change, the kinematic performance remained largely unaffected, requiring only minor adjustments to the robot's URDF (Unified Robot Description Format) model. A concurrent design priority was substantial weight reduction to improve the thrust-to-weight ratio and enhance aerial performance. Husky V2's mass characteristics are presented in Table 1, with comparative analysis to the Husky V3 prototype provided in Table 2, demonstrating the mass reduction achievements through design optimization and additive manufacturing refinement

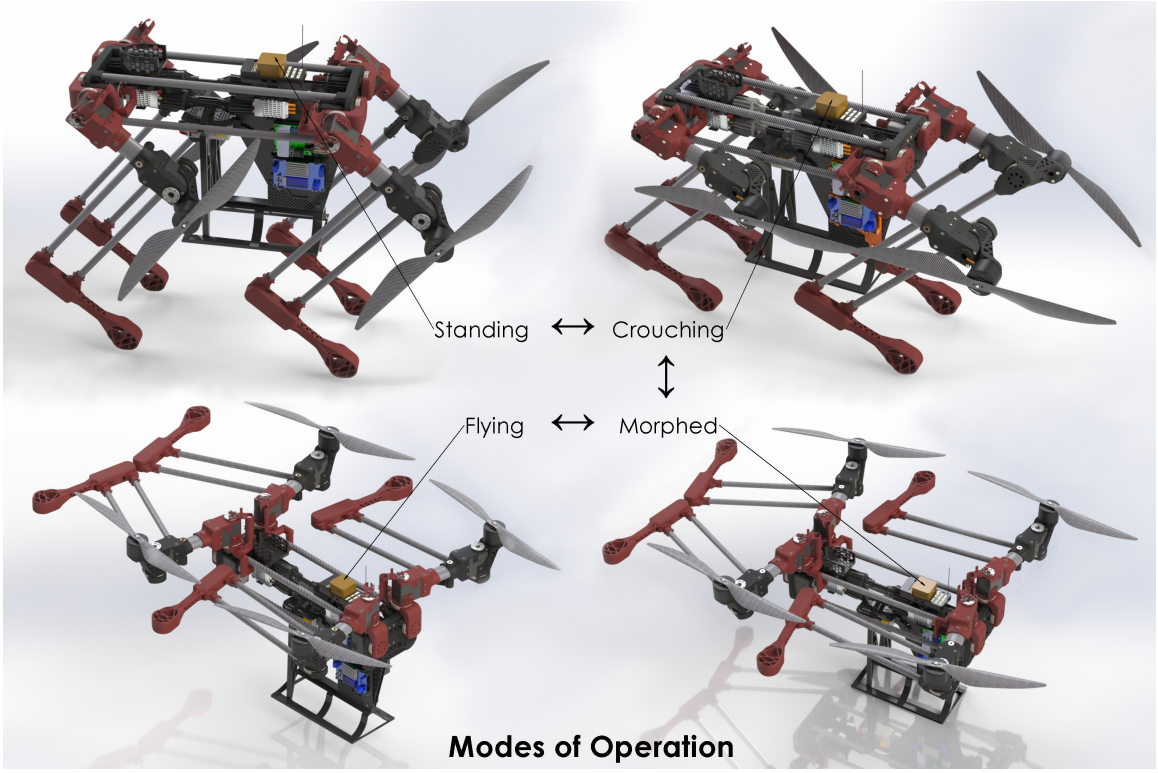

Figure 4.1: Shows the different modes of operation, which is also the sequencing of how the transition from Stance to aerial or reverse takes in action.

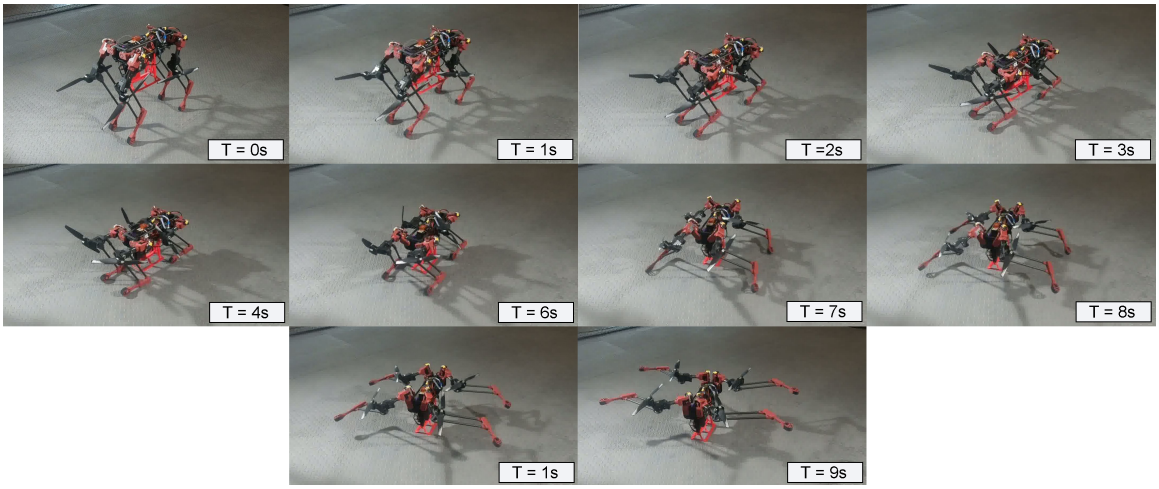

Figure 4.2: Morphing from Stance mode to Flight mode

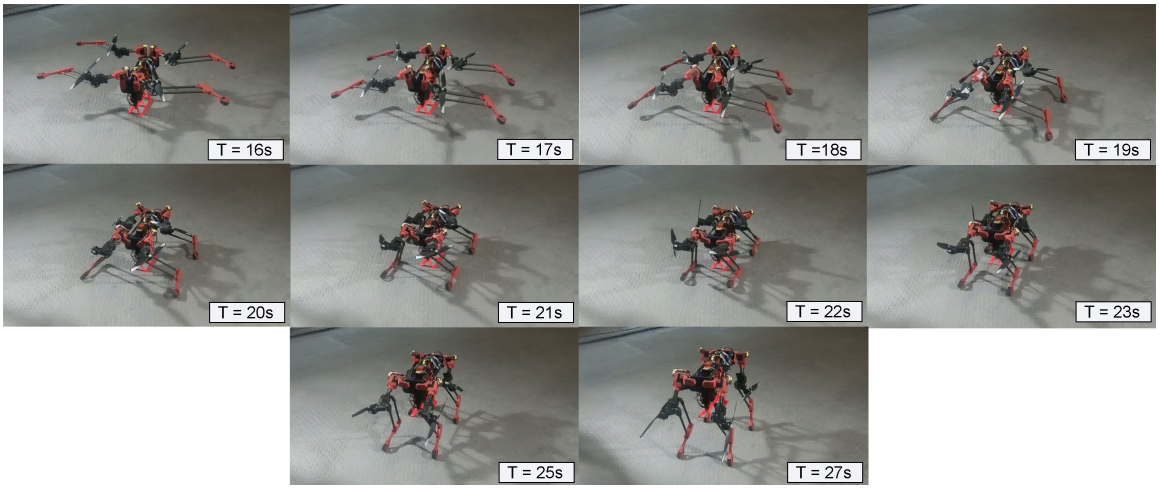

Figure 4.3: Morphing from Flight mode to Stance mode

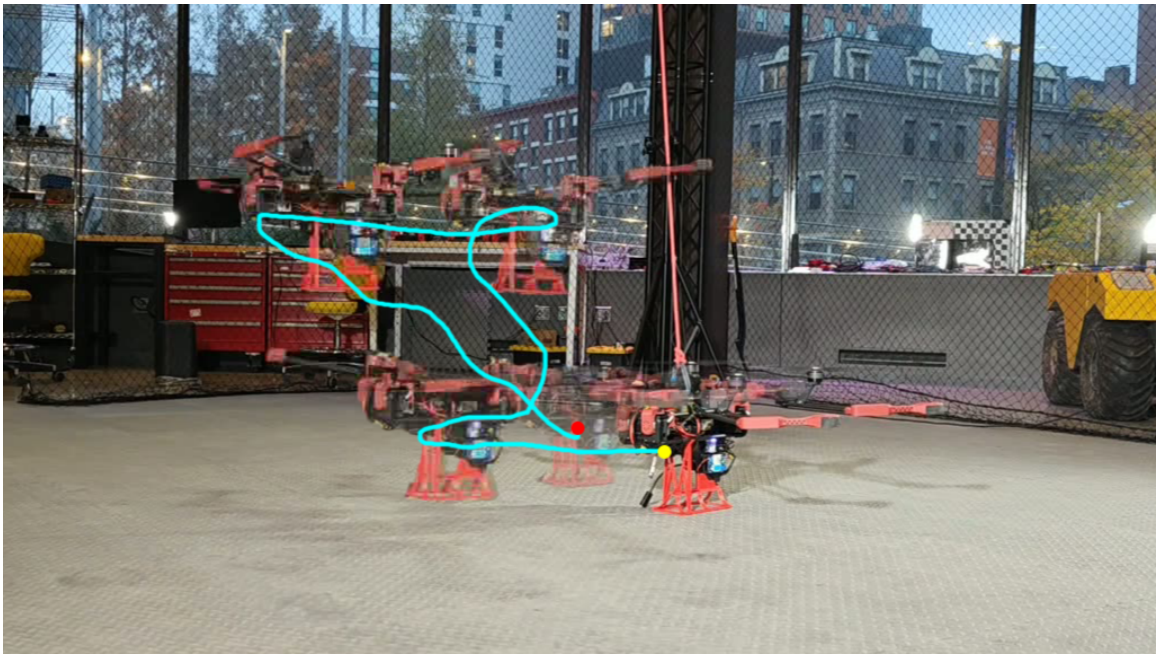

Figure 4.4: Shows the flight test with its path, yellow and red dots being the start and end position respectively.

Robot/Part	Body	Hip	Upper leg	Lower leg	Ankle	Foot	BLDC	Servos	Battery	Prop
Husky V2	2.335	0.033	0.733	0.060	0.053	0.075	0.197	0.165	0.500	0.021
Husky V3	2.240	0.025	0.674	0.032	0.035	0.025	0.197	0.165	0.500	0.021

Table 4.1: Component Mass Breakdown (KG).

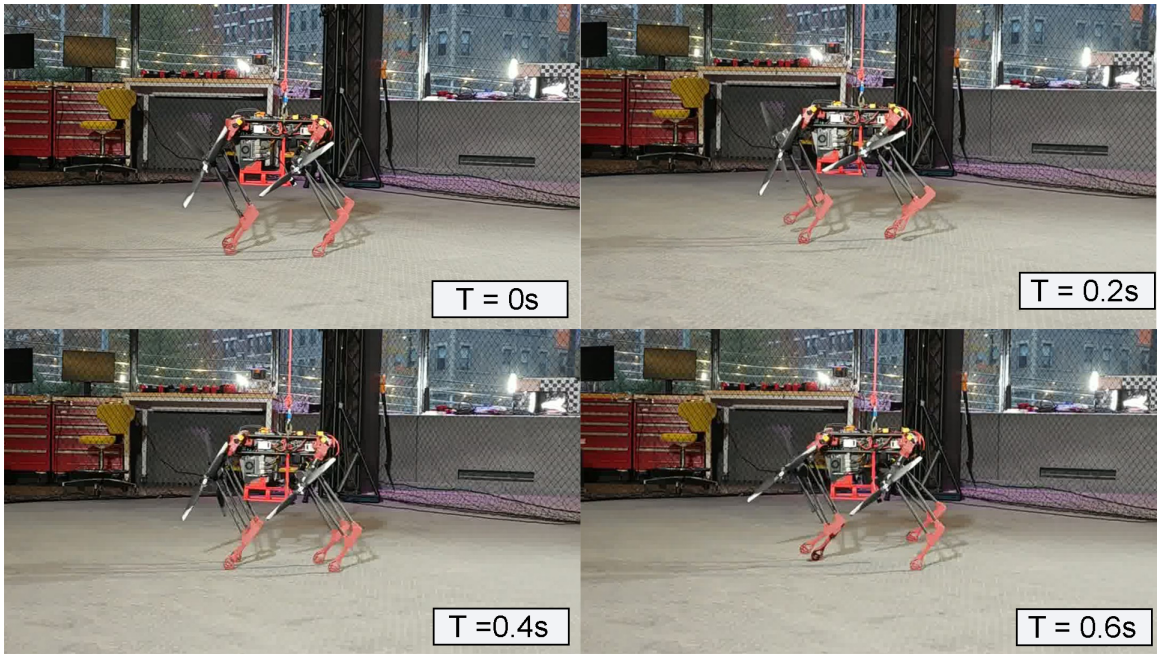

Figure 4.5: Shows the tethered trotting test for one gait cycle which is for $\tilde{0}$.4s.

4.2 Full CAD Model

This section presents:

1. Detailed location of the CAD model folder and access information.
2. Comprehensive list of all components.
3. Breakdown of all component weights (CAD estimations and experimental measurements).
4. Detailed list of subassemblies.

Item No.	Part Number	Description	Qty.	Weight
1	pelvisPlate_BB	Part of Torso	2	78
2	bodyTubeCF_BB	Carbon Fiber Tube 12x10x395mm	4	20.5
3	backBoneFrontConnector_BB	Backbone assembly	1	
4	backBoneBackConnector_BB	Backbone assembly	1	
5	backBoneBackPlate_BB	Carbon Fiber back bone plate	2	
6	backBoneFrontPlate_BB	Carbon Fiber back bone plate	2	
7	backBoneTubeConnector_BB	Backbone assembly	4	
8	backBoneTube_BB	Cabon fiber Tube 10x6x72mm	2	
9	perchV20.3_BB	Perch	1	135
10	XH540Torso_CC	Dynamixel XH540-W270-T with custom motor casing	4	170
11	mountESC_BB	front ESC mounting with pixhawk mount	1	20
12	mountESCBack_BB	Back ESC mounting with 4 way splitter	1	25
13	u2d2mounting_BB	Chest plate mounting for U2D2 and Voltage regulator	1	13
14	jetsonMounting_BB	Chest plate mounting for Jetson Nano	1	11
15	esc40A_BB	alpha 40A SEC	4	55
16	nvidiaJetsonNano_BB	Nvidia Jetson Nano computer	1	242
17	orangeCubePixhawk_BB	OranageCube Pixhawk FLight controller	1	34
18	u2duPowerHubBoard_BB	U2d2 Power hub board for power distribution and control	1	30
19	3pExtensionBoard_BB	Extension board for Star topology of dynamixels	1	10
20	tattu1300mahBattery_BB	22.2v 1300mah battery	1	240
21	voltageRegulatorZKJVA12KX_BB	Stepdown Voltage Regulator	1	55

Continued on next page...

Item No.	**Part Number**	**Description**	**Qty.**	
22	hipbone_HL	Hip bone	4	25
23	hipProximalConnector_UL	Supports bearing for Hip Sagittal motor	4	7
24	XH540Leg_CC	Dynamixel XH540-W270-T with custom motor casing	8	170
25	kneeDistalConnector_UL		4	25
26	hipDistalConnector_UL		4	28
27	femurBone_UL	Carbon Fiber Ellipse Bone	4	10
28	propMotor_UL	SUNNKSKY_X3515S	4	196
29	props15x5_HL	propellors 15x5cm	4	23
30	tibiaProximalConnector_LL		4	20
31	tibiaBone_LL		8	14.5
32	tibiaDistalConnector_LL		8	9
33	fibulaProximalConnector_LL		4	10
34	ankleBone_AL		4	50
35	bearing6806_CC		12	24
36	bearing694ZZ_CC		16	
37	B18.3.1M - 2.5 x 0.45 x 6 Hex SHCS – 6SHX	Wire Pipeline on ilder end	19	0.5
38	B18.3.1M - 3 x 0.5 x 30 Hex SHCS – 18SHX	HipDistal Connector	1	1
39	B18.3.1M - 3 x 0.5 x 12 Hex SHCS – 12SHX	Torso Assembly	8	1
40	B18.3.1M - 3 x 0.5 x 20 Hex SHCS – 20SHX	Leg Assembly	32	1
41	B18.3.1M - 3 x 0.5 x 25 Hex SHCS – 18SHX	Torso Assembly	10	1

Table 4.2: Bill of Materials

Chapter 5

Conclusion

This thesis has documented the mechanical design and development of Husky V3, advancing the Husky Carbon V2 platform through comprehensive refinement of structural components including the PIP articulated ankle, optimized torso architecture, and integrated wire routing. Iterative design methodology combined with additive manufacturing optimization has produced a lightweight, structurally rigid platform with improved thrust-to-weight ratio and operational reliability. Validation testing confirms robust performance across load conditions, demonstrating design viability for multi-modal locomotion and establishing Husky V3 as a practical platform for future legged-aerial robotic research.

The main achievement of this work was removing structural flexion from the torso and legs, which had caused problems with walking stability and flight control in earlier versions. By redesigning the body tube supports, strengthening the pelvis plate, and using optimized carbon fiber rods, the torso became much more rigid while still allowing some controlled movement for terrain adaptation. The print-in-place (PIP) articulated joints showed that 3D printing can create complex joints without needing assembly after printing, making manufacturing simpler. The redesigned motor casing with embedded bearings solved movement problems and created a clean wire routing system. Overall, these improvements show that careful iterative design produces robust, practical designs suitable for field-deployed robots.

In addition to structural improvements, Husky V3 became significantly lighter than Husky V2, which improved its power-to-weight ratio for better flight performance. Testing showed that ankle joints can withstand 23-25 kg of load without breaking and maintain flexibility through repeated cycles. The dual joint design in the ankle effectively distributes twisting forces, improving stability during transitions between ground and flight modes. Using standardized fasteners, lightweight

mounting brackets with snap-fit connections, and better thermal management for electronics shows that optimization improves the entire system, not just individual parts. These achievements demonstrate that Husky V3 is a practical, reliable platform for multimodal locomotion research.

Future work on the Husky V3 platform should focus on several key areas to advance the design further. Comprehensive field testing can identify structural weak points and fracture locations that may not have been revealed during laboratory validation, providing valuable data for next-generation refinement. The passive side of the motor can be optimized to absorb additional axial and radial loads, extending motor lifespan and improving overall performance reliability. The Fibula Proximal connector presents an opportunity for redesign using print-in-place (PIP) fabrication techniques, which would eliminate assembly complexity and reduce component weight while maintaining structural integrity. Additionally, continued optimization of additive manufacturing parameters and material selections can further reduce system mass without compromising performance. These improvements would advance Husky V3 toward a more refined, lighter, and more reliable multi-modal locomotion platform.

Bibliography

[1] Priyanshu Agarwal et al. “State Estimation for Legged Robots: Consistent Fusion of Leg Kinematics and IMU”. In: *Robotics: Science and Systems VIII*. MIT Press, 2013, pp. 17–24. ISBN: 978-0-262-31572-2. (Visited on 11/20/2025).

[2] Victor Barasuol et al. “A Reactive Controller Framework for Quadrupedal Locomotion on Challenging Terrain”. In: *2013 IEEE International Conference on Robotics and Automation*. 2013 IEEE International Conference on Robotics and Automation. May 2013, pp. 2554–2561. DOI: 10.1109/ICRA.2013.6630926. (Visited on 11/20/2025).

[3] Federico Bergonti, Matteo Ferraro, Giulio Di Franco, et al. “Co-Design Optimization Method for Morphing Drones Integrating Topology, Actuation, and Control”. In: *Proceedings of the 2024 IEEE International Conference on Robotics and Automation (ICRA)*. IEEE. Yokohama, Japan, May 2024.

[4] Niels Bucki and Mark T. Mueller. “Passive Morphing for Rapid Aerial Reconfiguration”. In: *Proceedings of the 2019 IEEE/RSJ International Conference on Intelligent Robots and Systems (IROS)*. IEEE. Macau, China, Nov. 2019.

[5] Pravin Dangol and Alireza Ramezani. “Feedback design for Harpy: a test bed to inspect thruster-assisted legged locomotion”. In: *Unmanned Systems Technology XXII*. Ed. by Hoa G. Nguyen, Paul L. Muench, and Charles M. Shoemaker. Vol. 11425. International Society for Optics and Photonics. SPIE, 2020, p. 1142507. DOI: 10.1117/12.2558284. URL: https://doi.org/10.1117/12.2558284.

[6] Pravin Dangol, Eric Sihite, and Alireza Ramezani. “Control of Thruster-Assisted, Bipedal Legged Locomotion of the Harpy Robot”. In: *Frontiers in Robotics and AI* Volume 8 - 2021 (2021). ISSN: 2296-9144. DOI: 10.3389/frobt.2021.770514. URL: https://www.frontiersin.org/journals/robotics-and%20ai/articles/10.3389/frobt.2021.770514.

[7] J. DiCarlo et al. “MIT Cheetah 3: Design and Control of a Robust, Dynamic Quadruped Robot”. In: *Proceedings of the 2018 IEEE/RSJ International Conference on Intelligent Robots and Systems (IROS)*. IEEE. 2018, pp. 6645–6651. DOI: 10.1109/IROS.2018.8593885.

[8] David Drotman et al. “Application-Driven Design of Soft, 3D Printed, Pneumatic Actuators with Bellows”. In: *IEEE/ASME Transactions on Mechatronics* 24.1 (Feb. 2019), pp. 78–87. ISSN: 1083-4435. DOI: 10.1109/TMECH.2018.2876161.

[9] Dylan Drotman et al. “Application-Driven Design of Soft, 3-D Printed, Pneumatic Actuators With Bellows”. In: *IEEE/ASME Transactions on Mechatronics* 24.1 (Feb. 2019), pp. 78–87. ISSN: 1941-014X. DOI: 10.1109/TMECH.2018.2879299. (Visited on 11/20/2025).

[10] Peter Fankhauser et al. “Robust Rough-Terrain Locomotion with a Quadrupedal Robot”. In: *2018 IEEE International Conference on Robotics and Automation (ICRA)*. 2018 IEEE International Conference on Robotics and Automation (ICRA). May 2018, pp. 5761–5768. DOI: 10.1109/ICRA.2018.8460731. (Visited on 11/20/2025).

[11] *Fully 3D-printed Soft Robots with Integrated Fluidic Circuitry — Science Advances*. https://www.science.o (Visited on 11/20/2025).

[12] Christian Gehring et al. “Dynamic Trotting on Slopes for Quadrupedal Robots”. In: *2015 IEEE/RSJ International Conference on Intelligent Robots and Systems (IROS)*. 2015 IEEE/RSJ International Conference on Intelligent Robots and Systems (IROS). Sept. 2015, pp. 5129–5135. DOI: 10.1109/IROS.2015.7354099. (Visited on 11/20/2025).

[13] Felix Grimminger et al. “An Open Torque-Controlled Modular Robot Architecture for Legged Locomotion Research”. In: *IEEE Robotics and Automation Letters* 5.2 (Apr. 2020), pp. 3650–3657. ISSN: 2377-3766, 2377-3774. DOI: 10.1109/LRA.2020.2976639. arXiv: 1910.00093 [cs]. (Visited on 11/20/2025).

[14] Felix Grimminger et al. “An Open Torque-Controlled Modular Robot Architecture for Legged Locomotion Research”. In: *IEEE Robotics and Automation Letters* 5.3 (July 2020), pp. 3650–3657. ISSN: 2377-3766. DOI: 10.1109/LRA.2020.2979660.

[15] Duncan Haldane et al. “Robotic Vertical Jumping Agility via Series-Elastic Power Modulation”. In: *Science Robotics* 1 (Dec. 2016), eaag2048. DOI: 10.1126/scirobotics.aag2048.

[16] Jonathan Hoff et al. “Synergistic Design of a Bio-Inspired Micro Aerial Vehicle with Articulated Wings”. In: *Robotics: Science and Systems 2016*. June 2016. DOI: 10.15607/RSS.2016.XII.009.

[17] Christian M. Hubicki et al. “A Systematic Comparison of Quadrupedal Robot Architectures”. In: *Proceedings of the 2014 IEEE International Conference on Robotics and Automation (ICRA)*. IEEE. Hong Kong, May 2014, pp. 3243–3250. DOI: 10.1109/ICRA.2014.6907393.

[18] Marco Hutter et al. “ANYmal - A Highly Mobile and Dynamic Quadrupedal Robot”. In: *Proceedings of the 2016 IEEE/RSJ International Conference on Intelligent Robots and Systems (IROS)*. IEEE. Daejeon, South Korea, Oct. 2016, pp. 38–44. DOI: 10.1109/IROS.2016.7758092.

[19] Fabian Jenelten et al. “Perceptive Locomotion in Rough Terrain – Online Foothold Optimization”. In: *IEEE Robotics and Automation Letters* 5.4 (Oct. 2020), pp. 5370–5376. ISSN: 2377-3766. DOI: 10.1109/LRA.2020.3007427. (Visited on 11/20/2025).

[20] Shuo Jiang et al. “Hierarchical RL-Guided Large-scale Navigation of a Snake Robot”. In: *2024 IEEE International Conference on Advanced Intelligent Mechatronics (AIM)*. 2024, pp. 1347–1352. DOI: 10.1109/AIM55361.2024.10637006.

[21] Shuo Jiang et al. “Snake Robot with Tactile Perception Navigates on Large-scale Challenging Terrain”. In: *2024 IEEE International Conference on Robotics and Automation (ICRA)*. 2024, pp. 5090–5096. DOI: 10.1109/ICRA57147.2024.10611384.

[22] Benjamin Katz et al. “Mini Cheetah: A Platform for Pushing the Limits of Dynamic Quadruped Control”. In: *Proceedings of the 2019 International Conference on Robotics and Automation (ICRA)*. IEEE. Montreal, Canada, May 2019, pp. 6295–6301. DOI: 10.1109/ICRA.2019.8793865.

[23] Galen Kenneally, Avik De, and Daniel E. Koditschek. “Kinematic Leg Design in an Electromechanical Robot”. In: *Proceedings of the 2014 IEEE International Conference on Robotics and Automation (ICRA)*. IEEE. Hong Kong, May 2014, pp. 4488–4495. DOI: 10.1109/ICRA.2014.6907520.

[24] Kyunam Kim et al. “A Bipedal Walking Robot That Can Fly, Slackline, and Skateboard”. In: *Science Robotics* 6.59 (Oct. 2021), eabf8136. DOI: 10.1126/scirobotics.abf8136. (Visited on 11/20/2025).

[25] Kyunam Kim et al. “A bipedal walking robot that can fly, slackline, and skateboard”. In: *Science Robotics* 6.59 (2021), eabf8136. DOI: 10.1126/scirobotics.abf8136. eprint: https://www.science.org/doi/pdf/10.1126/scirobotics.abf8136. URL: https://www.science.org/doi/abs/10.1126/scirobotics.abf8136.

[26] Kaushik Venkatesh Krishnamurthy et al. *Enabling steep slope walking on Husky using reduced order modeling and quadratic programming*. 2024. arXiv: 2411.11788 [cs.RO]. URL: https://arxiv.org/abs/2411.11788.

[27] Kaushik Venkatesh Krishnamurthy et al. *Optimization free control and ground force estimation with momentum observer for a multimodal legged aerial robot*. 2024. arXiv: 2411.11216 [cs.RO]. URL: https://arxiv.org/abs/2411.11216.

[28] Kaushik Venkatesh Krishnamurthy et al. “Thruster-Assisted Incline Walking of a Legged-Aerial Robot Using Reduced Order Model and Collocation Method”. In: *2025 American Control Conference (ACC)*. 2025, pp. 3738–3743. DOI: 10.23919/ACC63710.2025.11107924.

[29] Joonho Lee et al. “Learning Quadrupedal Locomotion over Challenging Terrain”. In: *Science Robotics* 5.47 (Oct. 2020), eabc5986. ISSN: 2470-9476. DOI: 10.1126/scirobotics.abc5986. arXiv: 2010.11251 [cs]. (Visited on 11/20/2025).

[30] Kaier Liang et al. “Rough-Terrain Locomotion and Unilateral Contact Force Regulations With a Multi-Modal Legged Robot”. In: *2021 American Control Conference (ACC)*. 2021, pp. 1762–1769. DOI: 10.23919/ACC50511.2021.9483189.

[31] Björn Lindqvist et al. “Multimodality Robotic Systems: Integrated Combined Legged-Aerial Mobility for Subterranean Search-and-Rescue”. In: *Robotics and Autonomous Systems* 154 (Aug. 2022), p. 104134. ISSN: 0921-8890. DOI: 10.1016/j.robot.2022.104134. (Visited on 11/20/2025).

[32] Ioannis Mandralis, Thibaut Tomic, and Marco Hutter. “ATMO: Smooth Ground-to-Aerial Transitions with Near-Ground Aerodynamics”. In: *IEEE Robotics and Automation Letters* 10.1 (Jan. 2025). ISSN: 2377-3766. DOI: 10.1109/LRA.2024.3522401.

[33] Ioannis Mandralis et al. “Minimum Time Trajectory Generation for Bounding Flight: Combining Posture Control and Thrust Vectoring”. In: *2023 European Control Conference (ECC)*. 2023, pp. 1–7. DOI: 10.23919/ECC57647.2023.10178360.

[34] Nir Meiri and David Zarrouk. "Flying Star: A Sprawl-Tuned Legged Robot with Aerial Capabilities". In: *IEEE Robotics and Automation Letters* 4.2 (Apr. 2019), pp. 1607–1613. ISSN: 2377-3766. DOI: 10.1109/LRA.2019.2897210.

[35] Takahiro Miki et al. "Learning Robust Perceptive Locomotion for Quadrupedal Robots in the Wild". In: *Science Robotics* 7.62 (Jan. 2022), eabk2822. ISSN: 2470-9476. DOI: 10.1126/scirobotics.abk2822. arXiv: 2201.08117 [cs]. (Visited on 11/20/2025).

[36] *Multi-Modal Mobility Morphobot (M4) with Appendage Repurposing for Locomotion Plasticity Enhancement — Nature Communications*. https://www.nature.com/articles/s41467-023-39018-y. (Visited on 11/20/2025).

[37] Arthur C. B. de Oliveira and Alireza Ramezani. "Thruster-assisted Center Manifold Shaping in Bipedal Legged Locomotion". In: *2020 IEEE/ASME International Conference on Advanced Intelligent Mechatronics (AIM)*. 2020, pp. 508–513. DOI: 10.1109/AIM43001.2020.9158967.

[38] Hojin Park, Joon Choi, and Junhyeong Lee. "Computational Design Towards Energy Efficient Optimization in Overconstrained Robotic Limbs". In: *Journal of Computational Design and Engineering* 10.5 (Sept. 2023), pp. 1847–1862. DOI: 10.1093/jcde/qwad083.

[39] Xue Bin Peng et al. "Sim-to-Real Transfer of Robotic Control with Dynamics Randomization". In: *2018 IEEE International Conference on Robotics and Automation (ICRA)*. May 2018, pp. 3803–3810. DOI: 10.1109/ICRA.2018.8460528. (Visited on 11/20/2025).

[40] Shreyansh Pitroda et al. "Capture Point Control in Thruster-Assisted Bipedal Locomotion". In: *2024 IEEE International Conference on Advanced Intelligent Mechatronics (AIM)*. 2024 IEEE International Conference on Advanced Intelligent Mechatronics (AIM). July 2024, pp. 1139–1144. DOI: 10.1109/AIM55361.2024.10637139. (Visited on 11/20/2025).

[41] Alireza Ramezani, Soon-Jo Chung, and Seth Hutchinson. "A biomimetic robotic platform to study flight specializations of bats". In: *Science Robotics* 2.3 (2017), eaal2505. DOI: 10.1126/scirobotics.aal2505. eprint: https://www.science.org/doi/pdf/10.1126/scirobotics.aal2505. URL: https://www.science.org/doi/abs/10.1126/scirobotics.aal2505.

[42] Alireza Ramezani and Eric Sihite. *Aerobat, A Bioinspired Drone to Test High-DOF Actuation and Embodied Aerial Locomotion*. 2022. arXiv: 2212.05361 [cs.RO]. URL: https://arxiv.org/abs/2212.05361.

[43] Alireza Ramezani et al. "Bat Bot (B2), a biologically inspired flying machine". In: *2016 IEEE International Conference on Robotics and Automation (ICRA)*. 2016, pp. 3219–3226. DOI: 10.1109/ICRA.2016.7487491.

[44] Adarsh Salagame, Eric Sihite, and Alireza Ramezani. *Validation of Tumbling Robot Dynamics with Posture Manipulation for Closed-Loop Heading Angle Control*. 2024. arXiv: 2411.12970 [cs.RO]. URL: https://arxiv.org/abs/2411.12970.

[45] Adarsh Salagame et al. "Crater Observing Bioinspired Rolling Articulator (COBRA)". In: *Advanced Intelligent Systems* (2025), p. 2500352. DOI: https://doi.org/10.1002/aisy.202500352.

[46] Adarsh Salagame et al. "Dynamic Posture Manipulation During Tumbling for Closed-Loop Heading Angle Control". In: *2024 IEEE International Conference on Advanced Intelligent Mechatronics (AIM)*. 2024, pp. 64–69. DOI: 10.1109/AIM55361.2024.10637168.

[47] Adarsh Salagame et al. "Heading Control for Obstacle Avoidance using Dynamic Posture Manipulation during Tumbling Locomotion". In: *2024 IEEE/RSJ International Conference on Intelligent Robots and Systems (IROS)*. 2024, pp. 13555–13560. DOI: 10.1109/IROS58592.2024.10801515.

[48] Adarsh Salagame et al. "How Strong a Kick Should be to Topple Northeastern's Tumbling Robot?" In: *2024 IEEE International Conference on Advanced Intelligent Mechatronics (AIM)*. 2024, pp. 76–81. DOI: 10.1109/AIM55361.2024.10637166.

[49] Adarsh Salagame et al. "NMPC-Based Unified Posture Manipulation and Thrust Vectoring for Fault Recovery". In: *IEEE Control Systems Letters* 9 (2025), pp. 2012–2017. DOI: 10.1109/LCSYS.2025.3589412.

[50] Adarsh Salagame et al. "Non-impulsive Contact-Implicit Motion Planning for Morpho-functional Loco-manipulation". In: *2024 IEEE International Conference on Advanced Intelligent Mechatronics (AIM)*. 2024, pp. 309–314. DOI: 10.1109/AIM55361.2024.10637029.

[51] Adarsh Salagame et al. *Reinforcement Learning-Based Model Matching to Reduce the Sim-Real Gap in COBRA*. 2024. arXiv: 2406.13700 [cs.RO]. URL: https://arxiv.org/abs/2406.13700.

[52] Adarsh Salagame et al. *Vision-Guided Loco-Manipulation with a Snake Robot*. 2025. arXiv: 2503.18308 [cs.RO]. URL: https://arxiv.org/abs/2503.18308.

[53] Abhishek Sebastian. *Soft Robotics for Search and Rescue: Advancements, Challenges, and Future Directions*. http://arxiv.org/abs/2502.12373. Feb. 2025. DOI: 10.48550/arXiv.2502.12373. arXiv: 2502.12373 [cs]. (Visited on 11/20/2025). Pre-published.

[54] Sangok Seok et al. "Design Principles for Energy-Efficient Legged Locomotion and Implementation on the MIT Cheetah Robot". In: *IEEE/ASME Transactions on Mechatronics* 20.3 (June 2015), pp. 1117–1129. ISSN: 1083-4435. DOI: 10.1109/TMECH.2015.2415052.

[55] E. Sihite, P. Kelly, and A. Ramezani. *Mechanism Design of a Bio-inspired Armwing Mechanism for Mimicking Bat Flapping Gait*. 2020. arXiv: 2010.04702 [cs.RO]. URL: https://arxiv.org/abs/2010.04702.

[56] Eric Sihite, Pravin Dangol, and Alireza Ramezani. "Unilateral Ground Contact Force Regulations in Thruster-Assisted Legged Locomotion". In: *2021 IEEE/ASME International Conference on Advanced Intelligent Mechatronics (AIM)*. 2021, pp. 389–395. DOI: 10.1109/AIM46487.2021.9517648.

[57] Eric Sihite, Peter Kelly, and Alireza Ramezani. "Computational Structure Design of a Bio-Inspired Armwing Mechanism". In: *IEEE Robotics and Automation Letters* 5.4 (2020), pp. 5929–5936. DOI: 10.1109/LRA.2020.3010217.

[58] Eric Sihite and Alireza Ramezani. "A morphology-centered view towards describing bats dynamically versatile wing conformations". In: *The International Journal of Robotics Research* 44.3 (2025), pp. 431–464. DOI: 10.1177/02783649241272132. eprint: https://doi.org/10.1177/02783649241272132. URL: https://doi.org/10.1177/02783649241272132.

[59] Eric Sihite and Alireza Ramezani. "Enforcing nonholonomic constraints in Aerobat, a roosting flapping wing model". In: *2020 59th IEEE Conference on Decision and Control (CDC)*. 2020, pp. 5321–5327. DOI: 10.1109/CDC42340.2020.9304158.

[60] Eric Sihite and Alireza Ramezani. *Wake-Based Locomotion Gait Design for Aerobat*. 2022. arXiv: 2212.05359 [cs.RO]. URL: https://arxiv.org/abs/2212.05359.

[61] Eric Sihite et al. *Bang-Bang Control Of A Tail-less Morphing Wing Flight*. 2022. arXiv: 2205.06395 [cs.RO]. URL: https://arxiv.org/abs/2205.06395.

[62] Eric Sihite et al. "Demonstrating Autonomous 3D Path Planning on a Novel Scalable UGV-UAV Morphing Robot". In: *2023 IEEE/RSJ International Conference on Intelligent Robots and Systems (IROS)*. 2023, pp. 3064–3069. DOI: 10.1109/IROS55552.2023.10342189.

[63] Eric Sihite et al. “Efficient Path Planning and Tracking for Multi-Modal Legged-Aerial Locomotion Using Integrated Probabilistic Road Maps (PRM) and Reference Governors (RG)”. In: *2022 IEEE 61st Conference on Decision and Control (CDC)*. 2022, pp. 764–770. DOI: 10.1109/CDC51059.2022.9992754.

[64] Aman Singh et al. “A Chain-Driven, Sandwich-Legged Quadruped Robot: Design and Experimental Analysis”. In: *arXiv preprint* 2503.14255 (Mar. 2025). Submitted to major robotics conference. URL: https://arxiv.org/abs/2503.14255.

[65] Yu Sun, Hao Zhao, and Weifeng Gao. “Topology Optimization for Monolithic Compliant Quadruped Legs”. In: *Mechanism and Machine Theory* 181 (Mar. 2023), pp. 105–122. DOI: 10.1016/j.mechmachtheory.2023.105148.

[66] Kyle L. Walker. “Design and Control of a Metamorphic Aerial Robot with Bi-Stable Morphing Arms”. In: *Proceedings of the 2023 IEEE International Conference on Robotics and Automation (ICRA)*. IEEE. London, UK, May 2023.

[67] Gustav Waltersson, Raffaella Laezza, and Yiannis Karayiannidis. “Planning and Control for Cable-Routing with Dual-Arm Robot”. In: *Proceedings of the 2022 International Conference on Robotics and Automation (ICRA)*. IEEE. Philadelphia, USA, May 2022, pp. 1046–1052. DOI: 10.1109/ICRA46639.2022.9811765.

[68] Chenghao Wang and Alireza Ramezani. *Thruster-Enhanced Locomotion: A Decoupled Model Predictive Control with Learned Contact Residuals*. 2025. arXiv: 2508.03003 [cs.RO]. URL: https://arxiv.org/abs/2508.03003.

[69] Chenghao Wang et al. *Dynamic Quadrupedal Legged and Aerial Locomotion via Structure Repurposing*. 2025. arXiv: 2510.09526 [cs.RO]. URL: https://arxiv.org/abs/2510.09526.

[70] Michael Wehner et al. “An Integrated Design and Fabrication Strategy for Entirely Soft, Autonomous Robots”. In: *Nature* 536.7617 (Aug. 2016), pp. 451–455. ISSN: 1476-4687. DOI: 10.1038/nature19100. (Visited on 11/20/2025).

[71] Michael Wehner et al. “An Integrated Design and Fabrication Strategy for Entirely Soft, Multifunctional Robots”. In: *Nature* 536.7617 (Aug. 2016), pp. 451–455. ISSN: 0028-0836. DOI: 10.1038/nature19100.

[72] Patrick M. Wensing et al. “Proprioceptive Actuator Design in the MIT Cheetah: Impact Mitigation and High-Bandwidth Physical Interaction for Dynamic Legged Robots”. In: *IEEE Transactions on Robotics* 33.6 (Dec. 2016), pp. 1289–1302. ISSN: 1552-3098. DOI: 10.1109/TRO.2016.2640183.

[73] Zhaoming Xie et al. *Iterative Reinforcement Learning Based Design of Dynamic Locomotion Skills for Cassie*. Mar. 2019. DOI: 10.48550/arXiv.1903.09537. arXiv: 1903.09537 [cs]. (Visited on 11/20/2025).

[74] Zhenishbek Zhakypov, Christoph H. Belke, and Jamie Paik. “Tribot: A Deployable, Self-Righting and Multi-Locomotive Origami Robot”. In: *2017 IEEE/RSJ International Conference on Intelligent Robots and Systems (IROS)*. 2017 IEEE/RSJ International Conference on Intelligent Robots and Systems (IROS). Sept. 2017, pp. 5580–5586. DOI: 10.1109/IROS.2017.8206445. (Visited on 11/20/2025).

[75] Jihong Zhu et al. “Dual-Arm Robotic Manipulation of Flexible Cables”. In: *Proceedings of the 2018 IEEE/RSJ International Conference on Intelligent Robots and Systems (IROS)*. IEEE. Madrid, Spain, Oct. 2018, pp. 3052–3059. DOI: 10.1109/IROS.2018.8593780.